

**An-Najah National University**  
**Faculty of Graduate Studies**

**Effects of the hydrostatic pressure and temperature on  
the properties of the (GaAs) single quantum dot in a  
magnetic field**

**By**  
**Faten Maher Bzour**

**Supervisor**  
**Prof. Mohammad Elsaid**

**Co-supervisor**  
**Dr. Khaled Ilaiwi**

**This Thesis is Submitted in Partial Fulfillment of the Requirements for  
the Degree of Master of Physics, Faculty of Graduate Studies, An-  
Najah National University, Nablus, Palestine.**

**2016**

**Effects of the Hydrostatic Pressure and Temperature  
on the Properties of the (GaAs) Single Quantum Dot in  
a Magnetic Field**

**By**

**Faten Maher Bzour**

**This thesis was defended successfully on 2/6/2016 and approved by:**

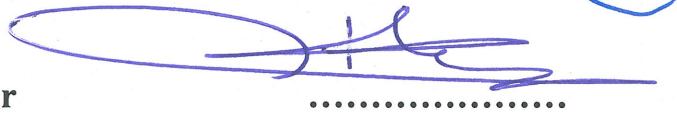
**Defense committee Members**

**Signature**

– Prof. Mohammad Elsaid /Supervisor

  
.....

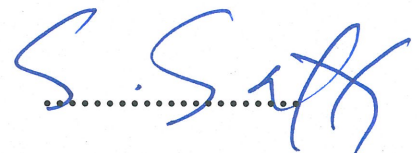
– Dr. Khaled Ilaiwi /Co-Supervisor

  
.....

– Prof. Atef Qassrawi /External Examiner

  
.....

– Prof. Ghassan Saffarini /Internal Examiner

  
.....

III

## **Dedication**

To my family

## **Acknowledgments**

First of all, thanks and praises to Allah for giving me strength and patience to complete this work.

I would like to express my gratitude to my supervisor and instructor Prof. Dr. Mohammed Elsaid for his invaluable support and unlimited help and guidance during this work. My deepest appreciation for Dr. Khalid Ilaiwi for his efforts in carefully reading and commenting on the revisions of this manuscript. Not forgetting to thank Mr. Ayham Anwar Shaer for his time and assistance in Mathematica program.

Finally, my words fail to express my love and very profound gratitude to my beloved family; my parents for all what they did and still doing for me and for their understanding and endless love, my brothers (Anas, Eyas and Mohammed), my sisters (Enas, Aseel, Ansam and Esraa) for their support and continuous encouragement throughout the years of my study and through the process of researching and writing this thesis, my fiancé(Hassan) for being there when I needed him and for giving me love and support. This accomplishment would not have been possible without them. Thank you all.

## الإقرار

أنا الموقع أدناه مقدم الأطروحة التي تحمل عنوان

### Effects of the hydrostatic pressure and temperature on the properties of the (GaAs) single quantum dot in a magnetic field

أقر بأن ما اشتملت عليه هذه الرسالة إنما هو نتاج جهدي الخاص, باستثناء ما تمت الإشارة إليه حيثما ورد, وأن هذه الرسالة ككل أو جزء منها لم يقدم من قبل لنيل أية درجة أو بحث علمي أو بحثي لدى أية مؤسسة تعليمية أو بحثية أخرى

#### Declaration

The work provided in this thesis, unless otherwise referenced, is the researcher's own work, and has not been submitted elsewhere for any other degree or qualification.

Student's name:

اسم الطالب : فائق ماهر محمد بزور

Signature:

التوقيع : فائق

Date:

التاريخ : ٢٠١٦ / ٦ / ٢

## Table of Contents

Dedication .....	III
Acknowledgments .....	IV
Declaration .....	V
Table of Contents .....	VI
List of Tables.....	VII
List of Figures .....	VIII
List of Symbols and Abbreviations.....	XII
Abstract .....	XIV
Chapter One.....	1
Introduction .....	1
1.1 Low dimensional semiconductors .....	1
1.2 Fabrication methods.....	2
1.3 Heterostructure and confinement potential.....	5
1.4 Quantum dots and real atoms.....	8
1.5 Literature survey .....	10
1.6 Research objectives.....	12
1.7 Outlines of thesis.....	13
Chapter Two.....	15
Theory .....	15
2.1 Quantum dot Hamiltonian.....	15
2.2 Exact diagonalization method.....	16
2.3 Effective-mass approximation .....	19
Chapter three .....	20
Results and discussion.....	20
Chapter four.....	48
Conclusion.....	48
References .....	50
Appendix .....	53
الملخص .....	ب

## List of Tables

No.	Table Captions	Page
<b>Table (1.1)</b>	comparison between QDs and atoms	<b>9</b>
<b>Table (3.1)</b>	The ground state energies of QD as a function of dimensionless parameter $\lambda$ obtained from exact diagonalization method (second column) compared with reported work (third column) Ref [3].	<b>21</b>
<b>Table (3.2)</b>	The energy of the QD states ( $m_r = 0, 1, 2, 3, 4$ ) versus the magnetic field for $\omega_o = \frac{2}{3} R^*$ (the shaded energy values show the transitions in the angular momentum of the ground state of the QD).	<b>25</b>
<b>Table (3.3)</b>	The energy of the QD states ( $m_r = 0, 1, 2, 3, 4$ ) versus the magnetic field for $\omega_o = 0.5 R^*$ (the shaded energy values show the transitions in the angular momentum of the ground state of the QD).	<b>26</b>
<b>Table (3.4)</b>	The exchange energy of the quantum dot versus the strength of the magnetic field for $\omega_o = \frac{2}{3} R^*$ , T = 0 K, P = 0 Kbar.	<b>31</b>

## List of Figures

No.	Figure Captions	Page
<b>Figure (1.1)</b>	Schematic image and the density of state as function of energy for various confinement systems: bulk (3D), quantum well (2D), quantum wire (1D), and quantum dot (0D).	<b>2</b>
<b>Figure (1.2)</b>	The assumed geometry of the (a) pyramidal and (b) lens-shaped quantum dots.	<b>4</b>
<b>Figure (1.3)</b>	Schematic picture for the mechanism of confining electrons in semiconductor QD heterostructure a) 2DEG at the interface between GaAs and AlGaAs heterostructure. The electrons in the 2DEG are due to the ionization of silicon donors located in the n-AlGaAs layer. b) The metal electrodes on the surface of heterostructure are used to apply a negative voltage in order to deplete locally the electrons below 2DEG. In this way, we can confine the electrons in zero dimensions to obtain a QD system.	<b>7</b>
<b>Figure (1.4)</b>	Quantum dot defined by metallic gate electrodes: (a) schematic view of the quantum dot (b) scanning electron micrograph of the metallic surface gates.	<b>8</b>
<b>Figure (1.5)</b>	The potential energy and discrete energy levels for the atom and for the quantum dot.	<b>9</b>
<b>Figure (3.1)</b>	(a): The computed energy spectra of quantum dot versus the strength of the magnetic field for $\omega_0 = \frac{2}{3} R^*$ , $T = 0$ K, $P = 0$ Kbar and angular momentum $m = 0, \pm 1, \pm 2, \pm 3$ . (b) the energy spectra from reported work (Ref [44])	<b>23</b>
<b>Figure (3.2)</b>	The computed energy spectra of quantum dot versus the strength of the magnetic field for $\omega_0 = 0.5R^*$ , $T = 0$ K, $P = 0$ Kbar and angular momentum $m = 0, 1, 2, 3, 4$ .	<b>24</b>
<b>Figure (3.3)</b>	The singlet-triplet phase diagram of the quantum dot. The magnetic field strength $\omega_c$ versus the confining frequency $\omega_0$ .	<b>27</b>
<b>Figure (3.4)(a)</b>	The exchange energy of the QD versus the	<b>29</b>



	magnetic field strength for $\omega_o = \frac{2}{3} R^*$ , $T = 0$ K, $P = 0$ Kbar.	
<b>Figure (3.4)(b)</b>	The exchange energy of the QD versus the magnetic field strength for $\omega_o = \frac{2}{3} R^*$ , $T = 0$ K, $P = 0$ Kbar from Ref [44]	<b>29</b>
<b>Figure (3.4)(c)</b>	The exchange energy of the QD versus the magnetic field strength for $\omega_o = \frac{2}{3} R^*$ , $T = 0$ K, $P = 0$ Kbar.	<b>30</b>
<b>Figure (3.5)</b>	The exchange energy of the QD versus the magnetic field strength for $\omega_o = 0.5 R^*$ , $T = 0$ K, $P = 0$ Kbar.	<b>30</b>
<b>Figure (3.6)</b>	The pressure and temperature static dielectric constant against the hydrostatic pressure at $T=0$ K.	<b>33</b>
<b>Figure (3.7)</b>	The pressure and temperature static dielectric constant against the temperature at $P = 0$ Kbar.	<b>33</b>
<b>Figure (3.8)</b>	The pressure and temperature electron effective mass against the pressure at $T = 0$ K.	<b>34</b>
<b>Figure (3.9)</b>	The pressure and temperature electron effective mass against the temperature at $P = 0$ Kbar.	<b>34</b>
<b>Figure (3.10)</b>	The computed energy spectra of quantum dot versus the strength of the magnetic field for $\omega_o = 0.5 R^*$ , $T = 0$ K, $P = 10$ Kbar and angular momentum $m_r = 0, 1, 2, 3, 4$ .	<b>35</b>
<b>Figure (3.11)</b>	The computed energy spectra of quantum dot versus the strength of the magnetic field for $\omega_o = 0.5 R^*$ , $T = 0$ K, $P = 20$ Kbar and angular momentum $m_r = 0, 1, 2, 3, 4$ .	<b>35</b>
<b>Figure (3.12)</b>	The computed energy spectra of quantum dot versus the strength of the magnetic field for $\omega_o = 0.5 R^*$ , $T = 0$ K, $P = 30$ Kbar and angular momentum $m_r = 0, 1, 2, 3, 4$ .	<b>36</b>
<b>Figure (3.13)</b>	The computed energy spectra of quantum dot versus the strength of the magnetic field for $\omega_o = 0.5 R^*$ , $T=0$ K, $m=0$ and various pressures ( $P = 0$ Kbar solid; $P = 10$ Kbar dashed; $P = 20$ Kbar dotted and $P = 30$ Kbar	<b>37</b>

	thick).	
<b>Figure (3.14)</b>	The exchange energy of the QD system versus the magnetic field strength for $\omega_o = 0.5 R^*$ , $T = 0$ K, $P = 10$ Kbar.	<b>38</b>
<b>Figure (3.15)</b>	The exchange energy of the QD system versus the magnetic field strength for $\omega_o = 0.5 R^*$ , $T = 0$ K, $P = 20$ Kbar.	<b>38</b>
<b>Figure (3.16)</b>	The exchange energy of the QD system versus the magnetic field strength for $\omega_o = 0.5 R^*$ , $T = 0$ K, $P = 30$ Kbar.	<b>39</b>
<b>Figure (3.17)</b>	The exchange energy of the QD system versus the magnetic field strength for $\omega_o = 0.5 R^*$ , $T = 0$ K and various pressures ( $P = 0$ Kbar solid; $P = 10$ Kbar dashed, $P = 20$ Kbar dotted and $P = 30$ Kbar thick).	<b>39</b>
<b>Figure (3.18)</b>	The computed energy spectra of quantum dot versus the strength of the magnetic field for $\omega_o = 0.5 R^*$ , $T = 150$ K, $P = 0$ Kbar and angular momentum $m_r = 0, 1, 2, 3, 4$ .	<b>40</b>
<b>Figure (3.19)</b>	The computed energy spectra of quantum dot versus the strength of the magnetic field for $\omega_o = 0.5 R^*$ , $T = 350$ K, $P = 0$ Kbar and angular momentum $m_r = 0, 1, 2, 3, 4$ .	<b>41</b>
<b>Figure (3.20)</b>	The energy of the quantum dot system versus the magnetic field strength for $\omega_o = 0.5 R^*$ , $P = 0$ Kbar, $m = 0$ and various temperatures ( $T = 0$ K solid, $T = 150$ K dashed and $T = 350$ K dotted).	<b>42</b>
<b>Figure (3.21)</b>	The exchange energy of the QD system versus the magnetic field strength for $\omega_o = 0.5 R^*$ , $T = 150$ K, $P = 0$ Kbar.	<b>43</b>
<b>Figure (3.22)</b>	The exchange energy of the QD system versus the magnetic field strength for $\omega_o = 0.5 R^*$ , $T = 350$ K, $P = 0$ Kbar.	<b>43</b>
<b>Figure (3.23)</b>	The exchange energy of the QD system versus the magnetic field strength for $\omega_o = 0.5 R^*$ , $P = 0$ Kbar and various temperatures ( $T = 0$ K solid; $T = 150$ K dashed $T = 350$ K dotted).	<b>44</b>
<b>Figure (3.24)</b>	The energy of the QD system against the hydrostatic pressure for $\omega_o = 0.5 R^*$ , $\omega_c = 0$	<b>45</b>

	$R^*$ $m_r = 0$ and various temperatures (T = 0 K solid; T = 150 K dashed; T = 350 K dotted).	
<b>Figure (3.25)</b>	The energy of the QD system against the temperature for $\omega_o = 0.5 R^*$ , $\omega_c = 0 R^*$ and various pressures (P = 0 Kbar solid; P = 2 Kbar dashed; P = 5 Kbar dotted and P = 7 Kbar dash-dotted).	<b>46</b>
<b>Figure (3.26)</b>	The computed energy of a two electron quantum dot for $m = 2$ , $\omega_c = 1 R^*$ and $\omega_o = 0.5 R^*$ , against the number of basis ( $s_p$ ) taken in diagonalization process.	<b>47</b>
<b>Figure (3.27)</b>	The computed energy of a two electron quantum dot for $m = 2$ , $\omega_c = 5 R^*$ and $\omega_o = 0.5 R^*$ , against the number of basis ( $s_p$ ) taken in diagonalization process.	<b>47</b>

## List of Symbols and Abbreviations

QD	Quantum dot
3D	Three dimension
2D	Two dimension
1D	One dimension
0D	Zero dimension (quantum dot)
$\mathcal{M}$	Magnetization
$I$	Current
A	Ampere
pA	Pico ampere
Sin	Spin Singlet state
Tri	Spin Triplet state
Sin-Tri	Singlet-triplet transition
$V_{SD}$	Source-Drain voltage
$V_g$	Gate voltage
$\omega_o$	Confining frequency
$\omega_c$	Cyclotron frequency
$B$	Magnetic field
$\chi$	Magnetic susceptibility
GaAs	Gallium Arsenide
AlGaAs	Aluminum Gallium Arsenide
MBE	Molecular beam epitaxy
n- AlGaAs	Negative type Aluminum Gallium Arsenide
2DEG	Two dimensional electron gas
$V(x,y)$	Lateral confinement potential
e	Charge of electron
m	Mass of electron
$m^*$	Effective mass of electron
$p(r)$	The linear momentum
R	Center of mass position
r	Relative motion position
$A(r)$	Vector potential
c	Speed of light
$\epsilon$	The dielectric constant of material
$R^*$	Effective Rydberg unit
$\hbar$	Reduced Blank's constant
$\alpha$	Effective frequency
$\nabla$	Gradient operator
$i$	Imaginary number
$\Psi$	Wave function

## XIII

K	Kelvin Degree
T	Temperature
n	Principle quantum number
m	Angular quantum number
S	Spin

**Effects of the hydrostatic pressure and temperature on the properties  
of the (GaAs) single quantum dot in a magnetic field**

**By**

**Faten Maher Bzour**

**Supervisor**

**Prof. Mohammad Elsaid**

**Co-supervisor**

**Dr. Khaled Ilaiwi**

**Abstract**

In the present work, we had calculated the energy levels of GaAs parabolic quantum dot under the combined effects of external pressure, temperature and magnetic field. The eigenenergies had been obtained by solving the two electron quantum dot Hamiltonian using the exact diagonalization method. The obtained results show that the energy levels of the quantum dot depend strongly on the pressure and temperature. We had found that the energy levels increase as the pressure enhances for fixed temperature and magnetic field and the quantum dot energy levels decrease as the temperature increases for fixed pressure and magnetic field. We had also computed the singlet-triplet phase diagram of the quantum dot. In addition, we had investigated the effect of the pressure on the magnetic field dependent exchange energy of the quantum dot. Finally, a comparative study to correlate the current foundations to previous works was carried out.

# Chapter One

## Introduction

### 1.1 Low dimensional semiconductors

Low dimensional systems are those systems in which one or more of the three dimensions is reduced to a length smaller than the Fermi wavelength, which result in the confinement of the electrons in one or more dimensions. The reduction of one dimension will result in a two-dimensional (2D) quantum well, reduction of two dimensions will result in a one dimensional (1D) quantum wire and eventually reduction of three dimensions produces a quantum dot (QD). As a result, some properties of these systems including the density of state and the energy spectra are changed. As presented in figure (1.1), the density of state for quantum dots is completely discrete and quantized due to its three dimensional confinement unlike the other confinements which have a continuous density of state [1, 2].

The size and shape of quantum dots can be experimentally tuned over a wide range resulting in a system with tunable electronic and physical properties [3], this unique parameter effects are impossible for bulk system. Generally, the diameter of QDs is about 100 nm.

The application of a magnetic field perpendicular to the dot plane will introduce an additional structure on the energy levels and correlation effects of the interacting electrons confined in a quantum dot.

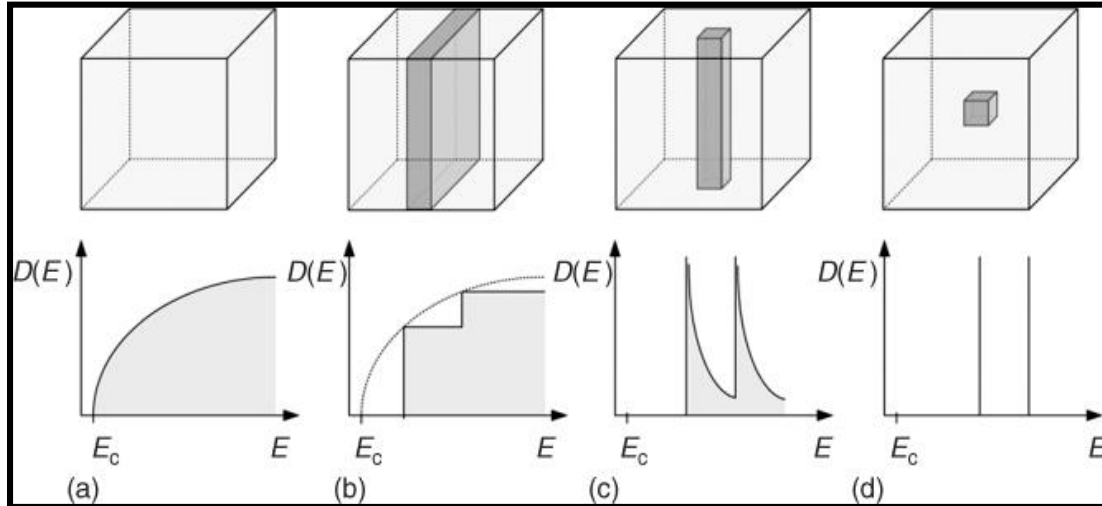


**Figure (1.11):** Schematic image and the density of state as function of energy for various confinement systems: bulk (3D), quantum well (2D), quantum wire (1D), and quantum dot (0D).

Due to their unique properties, quantum dots can be used in a variety of applications such as electronic devices including quantum dot lasers, single electron transistors [4], blue-laser diodes, solar cells and spin-based quantum computer [5-10].

Quantum dots can contain as less as one electron up to thousands of electrons, the number of electrons can be manipulated easily by conventional nanofabrication methods.

## 1.2 Fabrication methods

There are two ways to fabricate QDs. The first is called top-down approach which starts with a large scale objector pattern and gradually reduces its dimensions such as lithography technique. The second way is called bottom-up approach which depends on collecting and patterning atoms into the structure by chemical reactions such as the self-assembly method and chemical colloidal method.



Lithography technique is used to create two dimensional structures that can be etched down to form an isolated QD by using liquid acids or gas to dissolve away or remove unwanted material. Besides photolithography, there are large number of nanolithography methods including electron beam lithography, ion beam lithography, nanoimprint lithography, and dip pen nanolithography. Lithographic methods often produce contamination, defect formation, size non-uniformity, poor interface quality, and even damage to the bulk of the crystal itself [11]. It was also found that like photolithography and e-beam lithography are time-consuming and expensive processes, therefore there is a demand for other techniques for QDs fabrication [12].

Self-assembly method can be accomplished by two ways. One is called dip coating where the material is dipped in to a solution that chemically washes away all unwanted parts to form a film. The other method uses molecular-beam epitaxy or chemical vapor deposition to form the quantum dot arrays by depositing a semiconductor material with large lattice constant onto another semiconductor with smaller lattice constant under the theory of lattice mismatch. The resulting strain produces coherently strained islands on top of a two-dimensional wetting layer. These islands can be subsequently buried to form the quantum dot. Solar cell, light-emitting diodes, and capsule in drug delivery system are using this process to fabricate. In self-assembled QDs the structures are rather pyramidal or lens-shaped with sizes of approximately 10 nm as presented in figure (1.2) [13].

Chemical colloidal QD synthesis is based on rapid injection of semiconductor precursors into hot and stirred specific organic solvents containing molecules that can coordinate with the surface of the precipitated QD particles. QDs made with this method are used in biomedical applications [14, 15] and biotechnological applications such as biofunctional carrier spheres that are labeled with QDs.

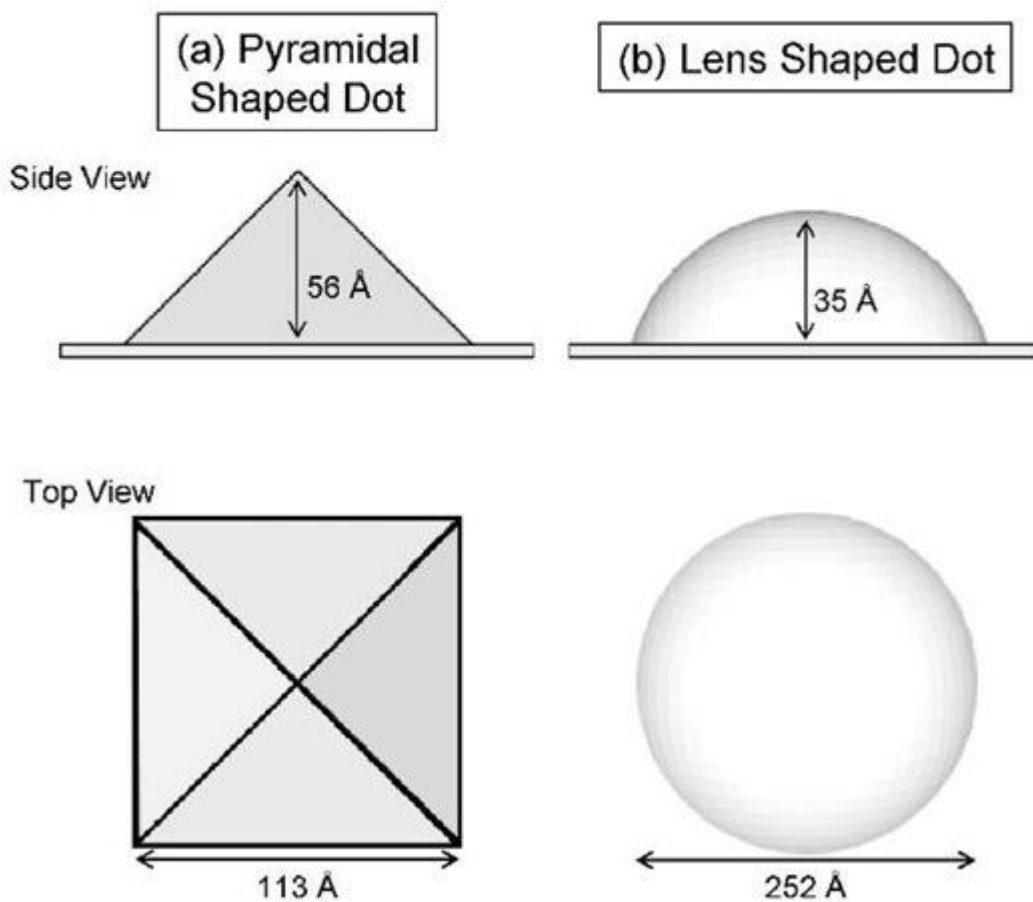


**Figure 1.2:** The assumed geometry of the (a) pyramidal and (b) lens-shaped quantum dots

### **1.3 Heterostructure and confinement potential**

QDs can be seen as small islands on a semiconductor heterostructure which result from confining the electrons in small regions of the order of nanometers. The shape of QDs and the number of the electrons can be controlled by artificial external potential.

In this research, the QD is made from GaAs/AlGaAs semiconductor heterostructure. The heterostructure is grown by using the molecular beam epitaxy (MBE) technique.

GaAs is composed from the element gallium (Ga) from column III and the element arsenic (As) from column V in the periodic table of elements. AlGaAs is obtained by substituting some of the Ga ions by aluminum (Al) ions, also from column III of the periodic table of elements.

GaAs has a high saturated electron velocity and high electron mobility. It also has a direct band gap, which means that it can be used to absorb and emit light efficiently. Such band gap results in a material that is resistance to radiation damage [16].

Both GaAs and AlGaAs have the same crystal structure but their band gaps are different. As a result, the grown layers are unstrained and sharp interfaces with reduced intermixing can be obtained. This allows extremely high performance, high electron mobility (compared to silicon MOSFETs and many other materials) and low electron density (compared to metal films). Nevertheless, these properties can be tuned in experiments with electric fields [16].

In figure 1.3, the n-AlGaAs layer (which is AlGaAs doped with silicon donors) is the source of free electrons in the heterostructure. These free electrons move from AlGaAs layer with high band gap to lower band gap GaAs layer. The electrons are trapped in the quantum well of GaAs layer. In this way the 2D structure where the motion of the electrons is quantized along growth axis (z direction) while the electron is free to move in x-y plane can be created.

As observed in figure 1.3(b), metal electrodes are deposited at the surface of the heterostructure through which a negative voltage is applied. As a result the confinement is further reduced and the electrons are confined to form one or more small islands in large two dimensional electron gas (2DEG).

The lateral confinement potential is usually taken to be a parabolic model; the theoretical-experimental comparisons show that harmonic oscillator model is the best to describe this confinement in postulates of quantum mechanics as the energy of the quantum dot is assumed to be conserved. Figure 1.4 shows the confinement potentials which were used to confine the electrons in a quantum dot [17].

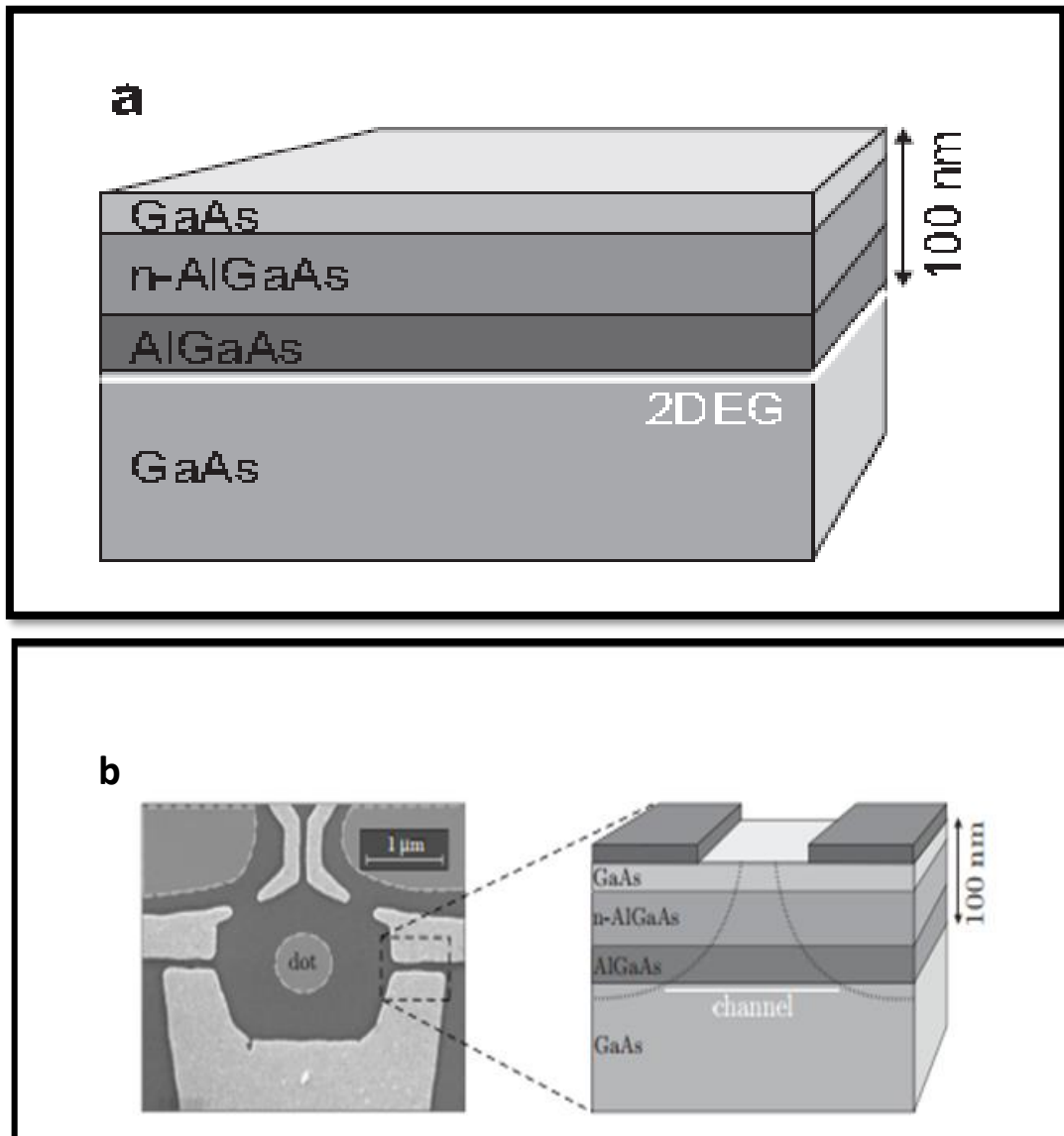


**Figure (1.3):** Schematic picture for the mechanism of confining electrons in semiconductor QD heterostructure a) 2DEG at the interface between GaAs and AlGaAs heterostructure. The electrons in the 2DEG are due to the ionization of silicon donors located in the n-AlGaAs layer. b) The metal electrodes on the surface of the heterostructure are used to apply a negative voltage in order to deplete locally the electrons below 2DEG. In this way, electrons are confined in zero dimensions to obtain a QD system.

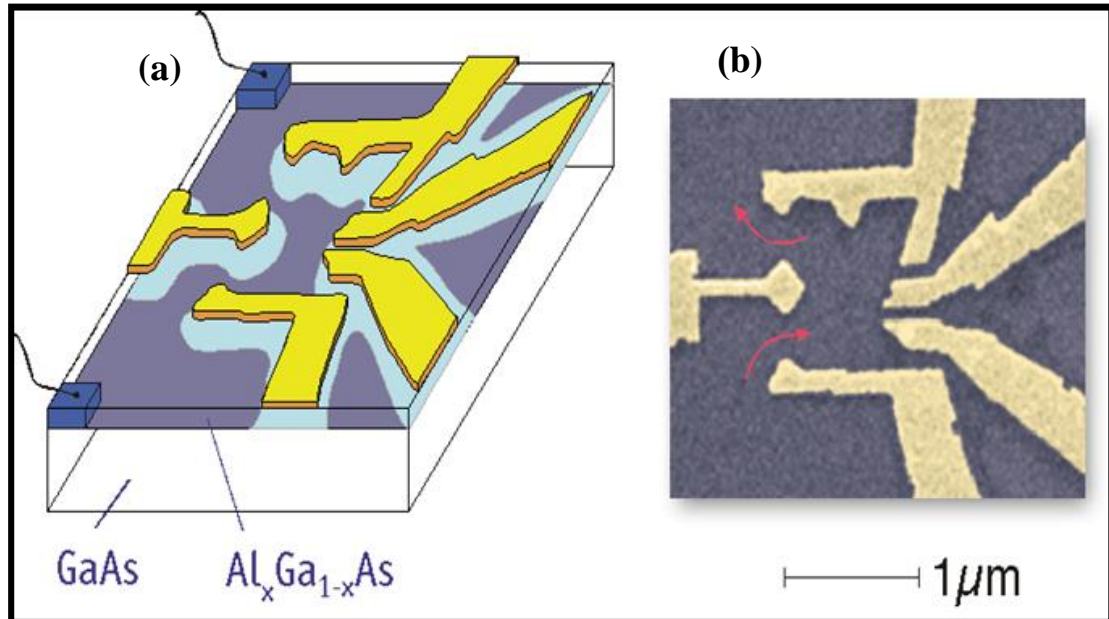


**Figure (1.4):** Quantum dot defined by metallic gate electrodes: (a) schematic view of the quantum dot (b) scanning electron micrograph of the metallic surface gates.

#### 1.4 Quantum dots and real atoms

In QDs electrons are trapped by a Lateral confinement potential resembling the columbic potential. The resembled columbic potential confines the electrons in real atoms, thus the energy spectrum of QDs becomes discrete like that of a real atom. As a result, QDs are called artificial atoms. Figure 1.5 shows the potential energy and discrete energy levels for the atom and for the quantum dot [18].

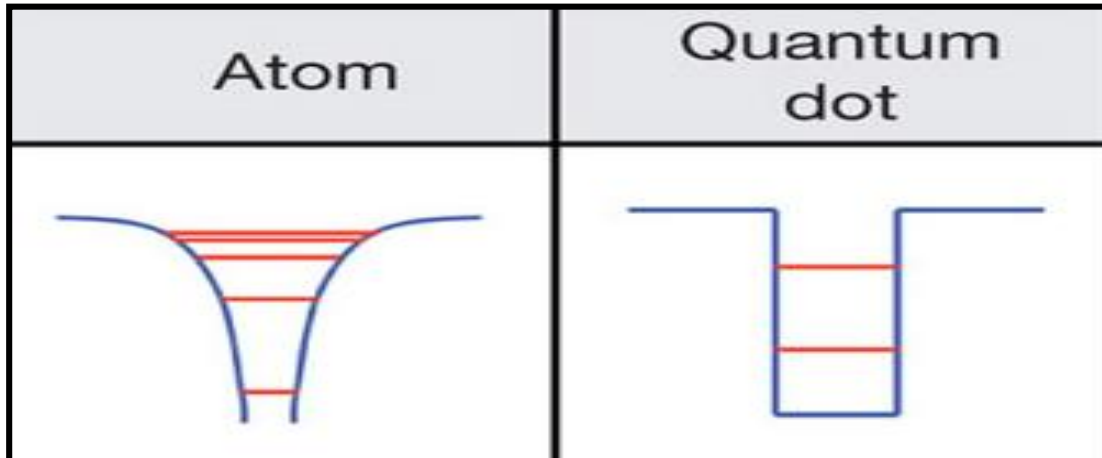


**Figure 1.5:** The potential energy and discrete energy levels for the atom and for the quantum dot.

The size of the QD is large and the separation between the energy levels is small compared to a real atom. This large size makes it possible to use a small magnetic field of a few Tesla to observe transitions that require a million Tesla to observe in real atoms.

The number of electrons in QD can be controlled by changing the applied potential while in real atoms by ionization. Moreover, in real atom electrons orbit the nucleus in 3D concentric shells but in QDs the orbits are 2D circles which mean that the number of electrons needed to fill each shell is different from real atoms. Table 1.1 shows the main differences between the real atom and QD [19].

**Table 1.1: Comparison between QDs and atoms**

parameter	atoms	Quantum dots
size	0.1 nm	100 nm
Level spacing	1 eV	0.1 eV
Ionization energy	10 eV	0.1 meV
Typical magnetic field	$10^4$ T	1-10 T

## 1.5 Literature survey

The physical properties of the quantum dot system are highly affected by the coulomb interaction and the electron-confinement interaction. The presence of the coulomb term makes the analytical solution for the Hamiltonian not available. Several theoretical methods were used to solve this problem [20-33]

Taut had studied the ground state spin oscillations of a two-electron quantum system by using the power series method to obtain an analytical solution [20]. Kandemir had applied variational method to study the two-electron quantum dot Hamiltonian by constructing trial wave functions from the quasi-exact analytic solution of the problem [21]. This Hamiltonian had been solved by Maksym and Chakraborty using exact diagonalization method to investigate the effect of the coulomb interaction on the energy spectrum. They calculated the heat capacity curve for both interacting and non-interacting confined electrons in the QD presented in a magnetic field. The interacting model showed very different behavior from non-interacting electrons, and the oscillations in these magnetic and thermodynamic quantities like magnetization ( $\mathcal{M}$ ) and heat capacity ( $C_v$ ) were attributed to the spin singlet-triplet transitions in the ground state spectra of the quantum dot [22]. Moreover, Ciftja had studied the ground state of two-dimensional quantum-dot helium in a zero magnetic field by using perturbation, diagonalization, and variational methods [3]. The quantum dot Hamiltonian had also been studied by Elsaid in different works using  $1/N$  expansion method to



investigate the electronic properties of two interacting electrons confined in a parabolic quantum dot under the influence of the applied magnetic field [23-29]. Among the theoretical methods, quantum Monte Carlo (QMC) method [30-32], and density functional theory method [33, 34] were used to solve this Hamiltonian. The magnetization, magnetic susceptibility and heat capacity of helium-like confined quantum dots have been calculated by De Groote et al, and an additional structure in the heat capacity was also obtained [35]. In a detailed study, Nguyen and Peeters [36] considered the QD in the presence of a single magnetic ion and applied magnetic field taking into account the electron-electron correlation in many electron quantum dot. They displayed the dependence of these thermal and magnetic quantities:  $C_v$ ,  $\mathcal{M}$  and  $\chi$  on the strength of the magnetic field, confinement frequency, magnetic ion position and temperature. They observed that the cusps in the energy levels show up as peaks in the heat capacity and magnetization.

Boyacioglu and Chatterjee had investigated the heat capacity and entropy effects for the quantum dot where the confinement is Gaussian instead of parabolic in the presence of a magnetic field by using the canonical ensemble approach [4]. Helle, Harju and Nieminen [37] computed the magnetization of a rectangular QD in a high magnetic field and the results showed the oscillation and smooth behavior in the magnetization curve for both, interacting and non-interacting confined electrons, respectively. The effects of pressure and temperature on the electronic and optical

properties of a quantum dot presented in external magnetic and electric fields had been considered very recently by many authors [38-42].

Rezaei et al. found that hydrostatic pressure and temperature have a great influence on the binding energy in a two dimensional QD [38] and spherical Gaussian QD [39]. Kirak et al. [40] studied the effects of the hydrostatic pressure and temperature on the binding energy and nonlinear optical properties for a QD with parabolic confinement. He found that the binding energy enhances by increasing pressure and decreases by temperature. Wen et al. [41] studied the external hydrostatic pressure influence on the electronic states and optical transitions of the InGaAs/GaAs QDs experimentally and theoretically. Sivakami et al. [42] studied the effect of hydrostatic pressure and temperature on coulomb interaction energy in the finite barrier model. The calculations were restricted to the singlet state.

This work will focus on the quantum dot system that consists of two electrons confined in a two dimensional parabolic potential in the presence of an external magnetic field and interacting by a Coulomb potential.

## **1.6 Research objectives**

The main aims of this research can be summarized as follows:

Firstly, the ground state energy of two dimensional quantum dot Hamiltonian in an external magnetic field will be studied using numerical exact diagonalization methods. The exchange energy ( $J$ ) of the QD

system will be calculated. The obtained results will be compared with previous studies [3, 42]. The computed ground state energy will be calculated as a function of the confinement frequency ( $\omega_0$ ) (the frequency of the potential that is used to reduce the 2DEG and confine the electrons in the QD) and the strength of the external magnetic field ( $\omega_c$ ).

Secondly, the effects of hydrostatic pressure (P) (hydrostatic means that the compression is isotropic, or equal in all three dimensions) and temperature (T) on the ground state energy and the exchange energy of the two dimensional quantum dot system will be investigated in the presence of an external magnetic field. The QDs may be subjected to pressure using a diamond anvil cell (DAC), and pressure measured using the photoluminescence of ruby loaded into the cell along with the sample, some gases such as condensed argon or nitrogen could be used as the pressure-transmitting medium in the DAC [41].

## **1.7 Outlines of thesis**

In this work, the effect of the temperature and pressure on the eigenenergies spectra of a quantum dot two electron atom in which both the magnetic field and the electron-electron interaction are fully taken into account have been discussed. Since, the eigenvalues of the electrons in the QD are the starting point to calculate the physical properties of the QD system, we had, first, applied the exact diagonalization method to solve the QD Hamiltonian and obtain the eigenenergies and the exchange

energy( $J$ ). Second, we had used the effective mass approximation to find effect of the temperature and pressure on the computed eigenenergies spectra of the QD as a function of magnetic field strength and confining frequency.

The rest of this thesis is organized as follows: the Hamiltonian theory, exact diagonalization technique and the effective mass approximation to find the effect of the temperature and pressure on the energy are presented in chapter II. In chapter III, the results of energy and the effect of the temperature and pressure on the properties of the quantum dot system had been displayed and discussed, while the final chapter is devoted for conclusions and future work.

## Chapter Two

### Theory

In this section the main three parts of the theory will be discussed in detail, namely: quantum dot Hamiltonian, exact diagonalization method and the effective-mass approximation.

#### 2.1 Quantum dot Hamiltonian

In this study the quantum dot system is composed of two electrons confined in a two dimensional parabolic potential in a uniform external magnetic field of strength  $B$ , applied along  $z$  direction. The interaction between the two electrons is considered to be purely coulombic. The Hamiltonian of this system can be written as:

$$\hat{H} = \sum_{j=1}^2 \left\{ \frac{1}{2m^*} \left[ \mathbf{p}(\mathbf{r}_j) + \frac{e}{c} \mathbf{A}(\mathbf{r}_j) \right]^2 + \frac{1}{2} m^* \omega_0^2 r_j^2 \right\} + \frac{e^2}{\epsilon |\mathbf{r}_1 - \mathbf{r}_2|} \quad (2.1)$$

Where  $m^*$  and  $\epsilon$  are defined as the effective mass and the dielectric constant for the GaAs medium, respectively.  $\omega_0$  is the angular frequency of the parabolic confining potential.  $\mathbf{r}_1$  and  $\mathbf{r}_2$  describe the positions of the two electrons in the  $x$ - $y$  plane.  $\mathbf{p}(\mathbf{r}_j)$  is the electron's 2D linear momentum operator and the symmetric gauge  $\mathbf{A} = \frac{1}{2} \mathbf{B} \times \mathbf{r}$  had been used.

The QD Hamiltonian can be separated into center of mass Hamiltonian ( $H_{CM}$ ) and relative Hamiltonian part ( $H_r$ ) as written below, the decoupling calculations are shown in details in appendix A.

$$\hat{H} = \hat{H}_{CM} + \hat{H}_r \quad (2.2)$$

The corresponding energy of this Hamiltonian equation (2.2) is:

$$E_{total} = E_{CM} + E_r \quad (2.3)$$

The center of mass Hamiltonian given by equation (A 11) is a harmonic oscillator type with well-known energies and wavefunction as shown in appendix A.

However, the relative motion Hamiltonian part ( $H_r$ ), given by equation (A 12) cannot be solved analytically for all ranges of  $\omega_0$  and  $\omega_c$ . In this work, exact diagonalization method will be used to solve the relative part of the Hamiltonian and obtain the corresponding eigenenergies ( $E_r$ ).

## 2.2 Exact diagonalization method

For non-interacting case the relative Hamiltonian in equation (A.12) can be reduced to a single particle problem with eigenstates  $|n_r m_r\rangle$  known as Fock-Darwin states [3] given by the following form,

$$|n_r m_r\rangle = N_{n_r m_r} \frac{e^{im_r \phi}}{\sqrt{2\pi}} (\alpha r)^{|m_r|} e^{-\alpha^2 r^2/2} L_{n_r}^{|m_r|}(\alpha^2 r^2), \quad (2.4)$$

Where  $n_r = 0, 1, \dots$  is the radial quantum number,  $m_r = 0, \pm 1, \pm 2, \dots$  is the angular momentum quantum number and  $L_{n_r}^{|m_r|}(\alpha^2 r^2)$  are the standard associated Laguerre polynomials. The normalization constant  $N_{n_r m_r}$  can be calculated from the normalization condition of the basis,  $\langle n_r m_r | n_r m_r \rangle = 1$ , to give:

$$N_{n_r m_r} = \sqrt{\frac{2n_r! \alpha^2}{(n_r + |m_r|)!}} \quad (2.5)$$

Where the absolute value of  $m_r$  ( $|m_r|$ ) is used to eliminate the negative values of  $m_r$  as the normalization constant should be real.

$\alpha$  is a constant which has the dimensionality of an inverse length given by:

$$\alpha = \sqrt{\frac{m\omega}{\hbar}} \quad (2.6)$$

$$\omega^2 = \frac{\omega_c^2}{4} + \omega_0^2 \quad (2.7)$$

$\omega_c$  is the cyclotron frequency which is used as a measure of the magnetic field strength and given by:

$$\omega_c = \frac{eB}{m^* c} \quad (2.8)$$

The eigenenergies of the QD Hamiltonian were given by equation (2.3) consist of the sum of the energies for the center of mass Hamiltonian ( $E_{cm}$ ) and the eigenenergies of the relative Hamiltonian part ( $E_r$ ). For interacting case, exact diagonalization method shall be applied to solve equation (A.12) and find the corresponding exact eigenenergies for arbitrary values of  $\omega_c$  and  $\omega_0$ .

The matrix element of the relative Hamiltonian part using the basis  $|n_r m_r\rangle$  can be expressed as,

$$\begin{aligned} h_{nn'} = \langle n_r, m_r | \hat{H}_r | n'_r, m_r \rangle = & \langle n_r m_r | -\frac{\hbar^2}{2\mu} \nabla^2 + \frac{1}{2} \mu \omega^2 r^2 | n'_r m_r \rangle \\ & + \langle n_r m_r | \frac{e^2}{\epsilon r} | n'_r m_r \rangle \end{aligned} \quad (2.9)$$

The corresponding relative dimensionless energies are,

$$\begin{aligned} E_r / \hbar\omega_0 = h_{nn'} / \hbar\omega_0 = & [(2n + |m_z| + 1) \sqrt{\left(1 + \frac{\gamma^2}{4}\right)} - \frac{\gamma}{2} m_z] \delta_{nn'} + \\ & \frac{\lambda}{\sqrt{2}} \sqrt{\frac{n'!n!}{(n'+|m_z|)! (n+|m_z|)!}} \times I_{nn'} |m_z| \end{aligned} \quad (2.10)$$

Where:

$$\gamma = \frac{\omega_c}{\omega_0} \quad (2.11)$$

$$\lambda = \frac{e^2 \alpha}{\hbar \omega_0} \quad (2.12)$$

are dimensionless parameters.  $\lambda$  gauges the strength of the coulomb energy to the confinement energy.

By direct substitution to  $r = \frac{\sqrt{t}}{\alpha}$  in the integration  $I_{nn'} = I_{n_r n'_r}$ , the coulomb energy matrix element can be expressed as:

$$\langle n_r m_r | \frac{e^2}{\epsilon r} | n'_r m_r \rangle \propto I_{nn'|m_z|} = \int_0^\infty dt t^{|m_z|} e^{-t} L_n^{|m_z|}(t) L_{n'}^{|m_z|}(t) \frac{1}{\sqrt{t}} \quad (2.13)$$

The above coulomb energy matrix element had been evaluated in a closed form by using the Laguerre relation [43] given in appendix B.

This closed form result of the coulomb energy reduces greatly the computation time needed in the diagonalization process.

In our calculation, the basis  $|n_r m_r\rangle$  defined by equation (2.4) had been used to diagonalize the relative QD Hamiltonian and obtain its corresponding eigenenergies ( $E_r$ ).

Having obtained the eigenenergies for the QD system for any state labeled by  $n, m$  quantum number, now we are able to calculate the exchange energy ( $J$ ) which is defined as:

$$J = E_{tri} - E_{sin} \quad (2.14)$$

Where  $E_{tri}$  is the energy of the lowest lying triplet and  $E_{sin}$  is the energy of the lowest lying singlet.



### 2.3 Effective-mass approximation

The effective mass approximation is used to study the effect of the pressure (P) and temperature (T) on the ground state energy. The Hamiltonian is given as follows.

$$\hat{H}(\vec{r}_1, \vec{r}_2) = \sum_{j=1}^2 \left\{ \frac{1}{2m^*(P,T)} \left[ \vec{p}(\vec{r}_j) + \frac{e}{c} \vec{A}(\vec{r}_j) \right]^2 \right\} + \frac{1}{2} m^*(P,T) \omega_0 r_j^2 + \frac{e^2}{\epsilon_r(P,T) |\vec{r}_1 - \vec{r}_2|} \quad (2.15)$$

Where  $\epsilon_r(P, T)$  and  $m^*(P, T)$  are the pressure and temperature dependent static dielectric constant and electron effective mass. For quantum dot made of GaAs  $\epsilon_r(P, T)$  and  $m^*(P, T)$  are given in appendix C: [38]

The pressure and temperature effective Rydberg ( $R_y^*(P, T)$ ) is used as the energy unit and given as follows:

$$R_y^*(P, T) = \frac{e^2}{2\epsilon(P,T)a_B^*(P,T)} \quad (2.16)$$

Where  $a_B^*(P, T)$  is the effective Bohr radius and given as:

$$a_B^*(P, T) = \epsilon(P, T) \hbar^2 / (m^*(P, T) e^2) \quad (2.17)$$

So the effective Rydberg can be written as:

$$R_y^*(P, T) = \frac{e^4 m^*(P, T)}{2(\epsilon(P, T))^2 \hbar^2} \quad (2.18)$$

The pressure and temperature values will be varied to study their effects on the ground state energy of the quantum dot Hamiltonian in a zero ( $\omega_c = 0$ ) and finite magnetic field ( $\omega_c$ ). Eventually, the ground state energies of the quantum dot system will be computed as function of temperature (T), pressure (P), confining frequency ( $\omega_0$ ) and magnetic field ( $\omega_c$ ). The obtained results are displayed in the next chapter.

## Chapter three

### Results and discussion

For two electrons in a parabolic GaAs quantum dot the effects of the hydrostatic pressure and temperature on the energy were computed and results are presented in this chapter. The physical parameters used for numerical calculations are: the dielectric constant ( $\epsilon = 12.74$ ), effective Rydberg ( $R^* = 5.825 \text{ meV}$ ) and the effective mass of an electron ( $m^* = 0.067 m_e$ ) at zero temperature and pressure [38].

Table 3.1 shows the ground state energy of the two interacting electrons for given values of  $\lambda$  (first column), defined by equation 2.12, assuming zero temperature, pressure and magnetic field. The results show excellent agreement between our obtained results (second column) and the results taken from Ref. [3] (third column) for all  $\lambda$ 's under consideration. The  $T=0 \text{ K}$ ,  $P = 0 \text{ Kbar}$ ,  $\omega_c = 0 R^*$  condition is assumed in quantum mechanics to ensure non spontaneous emission from ground state.

In figure 3.1 (a) the computed energy results for the two interacting electrons had been plotted against the magnetic field strength ( $\omega_c$ ) in the absence of pressure and temperature ( $P = 0 \text{ Kbar}$ ,  $T = 0 \text{ K}$ ) at  $\left(\omega_0 = \frac{2}{3} R^*\right)$ . Figure 3.1 (b) presents the energy results for  $\left(\omega_0 = \frac{2}{3} R^*\right)$  taken from Ref.[44]. The comparison between figures 3.1(a) and 3.1(b) show that our results agree very well with reported work.

**Table 3.1: The ground state energies of QD as a function of dimensionless parameter  $\lambda$  obtained from exact diagonalization method (second column) compared with reported work (third column) Ref [3].**

$\lambda$	E(present work)	E(Ref [3])
0	2.00000	2.00000
1	3.000969	3.00097
2	3.721433	3.72143
3	4.318718	4.31872
4	4.847800	4.84780
5	5.332238	5.33224
6	5.784291	5.78429
7	6.211285	6.21129
8	6.618042	6.61804
9	7.007949	7.00795
10	7.383507	7.38351

These figures show clearly the angular momentum transitions in the ground state of the quantum dot as the magnetic field rises. These transitions correspond to the (singlet-triplet) transitions.

Singlet-triplet transitions result from the combination of two reasons. First, because of the term  $-\frac{\gamma}{2}m_z$  in equation (2.10), the ( $m_r=0$ ) and ( $m_r = -1, -2, \dots$ ) energy levels rise in energy while levels with positive  $m_r$  ( $m_r = 1, 2, \dots$ ) drop in energy as seen in figure 3.1. Second, the coulomb interaction that acts stronger on singlets than on triplets as in singlets the electrons are closer according to Pauli principle. Thereby the gap between singlet and constitutive triplet is reduced. This leads to a sequence of different ground states ( $m_r = 0, 1, 2, \dots$ ) as the magnetic field increase. Since the total spin of the electron is ( $S = [1 - (-1)^m]/2$ ), the states

with even  $m$  are singlets whereas the states with odd  $m$  are triplets, which leads to singlet-triplet transition.

In all the next figures, only positive  $m_r$  energy levels are considered as they can be ground states unlike the negative  $m$  energy levels which rise in energy.

Figure 3.2 shows the computed energy results for the QD system versus the magnetic field strength ( $\omega_c$ ) in the absence of pressure and temperature ( $P = 0$  Kbar,  $T = 0$  K) at ( $\omega_0 = 0.5 R^*$ ). As seen in figure 3.2, at zero  $\omega_c$  the level ( $m_r = 1$ ) is higher in energy than ( $m_r = 0$ ) level, as  $\omega_c$  increases, ( $m_r = 1$ ) level drops in energy while the level ( $m_r = 0$ ) rises until their energy is equal at ( $\omega_c = 0.4 R^*$ ). At this point the electron makes transition from the singlet ( $m_r = 0$ ) energy level to the triplet ( $m_r = 1$ ) level and this is the first singlet- triplet transition point in table 3.3. The second transition point from ( $m_r = 1$ ) to ( $m_r = 2$ ) occur at  $\omega_c = 1.4 R^*$ . At  $\omega_c = 2.2 R^*$  and  $\omega_c = 3R^*$  the electron makes transition from ( $m_r = 2$ ) to ( $m_r = 3$ ) and from ( $m_r = 3$ ) to ( $m_r = 4$ ) respectively. Theses transition points correspond to the crossing points in the exchange energy graph.

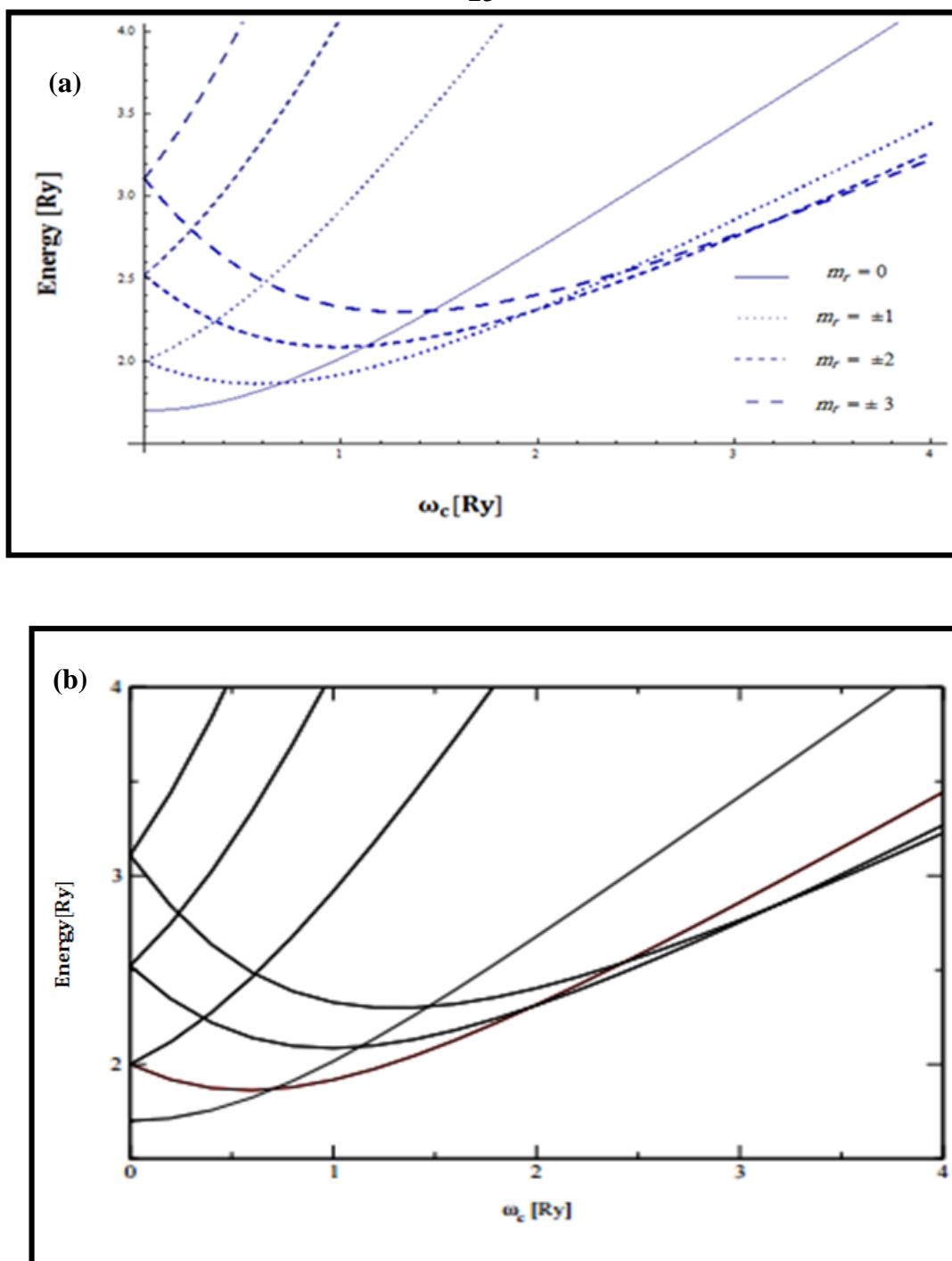


**Figure (3.1)** (a): The computed energy spectra of the quantum dot versus the strength of the magnetic field for  $\omega_0 = \frac{2}{3}R^*$ ,  $T = 0$  K,  $P = 0$  Kbar and angular momentum  $m_r = 0, \pm 1, \pm 2, \pm 3$ . (b) The energy spectra from reported work (Ref [44])

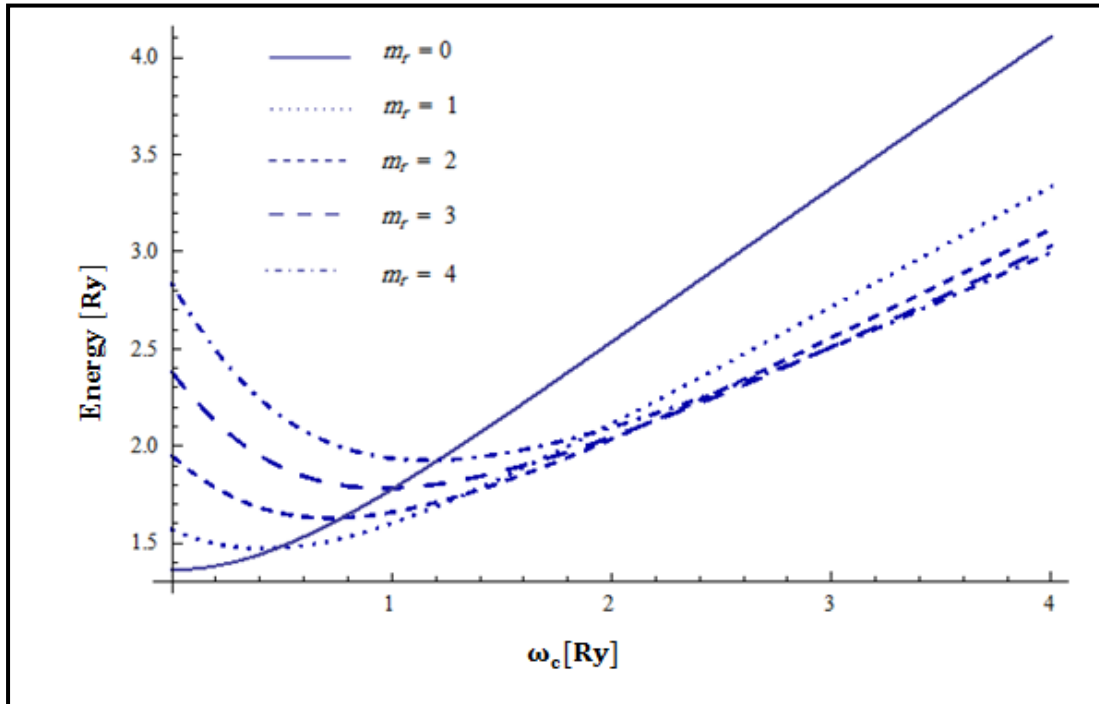


**Figure (3.2):** The computed energy spectra of the quantum dot versus the strength of the magnetic field for  $\omega_0 = 0.5 R^*$ ,  $T = 0$  K,  $P = 0$  Kbar and angular momentum  $m_r = 0, 1, 2, 3, 4$ .

In addition, the energy results of the QD system for ( $\omega_0 = \frac{2}{3} R^*$ ) and ( $\omega_0 = 0.5 R^*$ ) had been displayed in table 3.2 and 3.3 respectively. The angular momentum transitions as the magnetic field value rises are clearly noticed.

**Table (3.2): The energy of the QD states ( $m_r = 0, 1, 2, 3, 4$ ) versus the magnetic field for  $\omega_o = \frac{2}{3} R^*$  (the shaded energy values show the transitions in the angular momentum of the ground state of the QD).**

$\omega_c[\text{Ry}]$	$m_r = 0$	$m_r = 1$	$m_r = 2$	$m_r = 3$	$m_r = 4$
0	<b>1.69891</b>	2.00014	2.52193	3.10833	3.72267
0.2	1.71352	1.91905	2.34732	2.84068	3.36217
0.4	1.75622	1.87444	2.22178	2.63558	3.07805
0.6	1.82399	1.86272	2.14064	2.48721	2.86328
0.8	1.91275	<b>1.87899</b>	2.09757	2.38761	2.70824
1	2.01822	1.91809	2.08584	2.32833	2.60269
1.2	2.13655	1.97528	2.09923	2.30155	2.53712
1.4	2.2645	2.04659	2.13249	2.30058	2.50342
1.6	2.39955	2.12879	2.18132	2.32002	2.49499
1.8	2.53975	2.21941	2.24239	2.35558	2.50659
2	2.68364	2.31652	<b>2.31308</b>	2.40392	2.53414
2.2	2.83014	2.41866	2.3914	2.46248	2.57448
2.4	2.97845	2.52472	2.4758	2.52924	2.62515
2.6	3.12795	2.63385	2.56507	2.60265	2.68423
2.8	3.27821	2.74538	2.65829	2.68149	2.7502
3	3.42889	2.85879	2.75471	2.7648	2.82187
3.2	3.57975	2.97371	2.85376	<b>2.8518</b>	2.89829
3.4	3.73059	3.0898	2.95497	2.94189	2.97869
3.6	3.88129	3.20683	3.05798	3.03458	3.06246
3.8	4.03174	3.3246	3.16248	3.12945	3.14908
4	4.18187	3.44294	3.26822	3.22618	3.23815

**Table (3.3): The energy of the QD states ( $m_r = 0, 1, 2, 3, 4$ ) versus the magnetic field for  $\omega_o = 0.5 R^*$  (the shaded energy values show the transitions in the angular momentum of the ground state of the QD).**

$\omega_c[\text{Ry}]$	$m_r = 0$	$m_r = 1$	$m_r = 2$	$m_r = 3$	$m_r = 4$
0	<b>1.36265</b>	1.57099	1.94944	2.38114	2.83635
0.2	1.38322	1.49688	1.78376	2.1246	2.48923
0.4	1.4422	<b>1.4714</b>	1.6827	1.95	2.24188
0.6	1.5328	1.48663	1.63616	1.84478	2.07919
0.8	1.64702	1.53313	1.63206	1.79389	1.983
1	1.77774	1.60242	1.65943	1.78359	1.93669
1.2	1.91952	1.68789	1.7096	1.80298	1.92704
1.4	2.0685	1.78473	<b>1.77623</b>	1.84401	1.94427
1.6	2.22203	1.88958	1.85478	1.90092	1.98131
1.8	2.37834	2.00008	1.94206	1.96959	2.03316
2	2.53624	2.11461	2.03581	2.04711	2.0962
2.2	2.69491	2.23202	2.1344	<b>2.13137</b>	2.16784
2.4	2.85384	2.35149	2.23666	2.22081	2.24615
2.6	3.01264	2.47243	2.34174	2.31432	2.32973
2.8	3.17107	2.59442	2.44898	2.41103	2.41751
3	3.32898	2.71715	2.55792	2.51029	<b>2.50866</b>
3.2	3.48626	2.84038	2.66817	2.6116	2.60256
3.4	3.64283	2.96394	2.77947	2.71457	2.69872
3.6	3.79866	3.08769	2.89158	2.8189	2.79674
3.8	3.95373	3.21154	3.00434	2.92435	2.8963
4	4.10803	3.33541	3.1176	3.03071	2.99717



From figure 3.1 (a), figure 3.2, table 3.2 and table 3.3, it is noticed that as  $\omega_0$  rises the transition points are shifted towards higher values of  $\omega_c$ . This can be explained by noting that as  $\omega_0$  increase, the confinement of electrons increases and thus the quantum dot size decreases. Thereby the energy spacing between states increases and the electrons need more energy to make the transition so the transition happens at larger  $\omega_c$  value. The dependence of the angular momentum on the confinement frequency is shown in figure 3.3

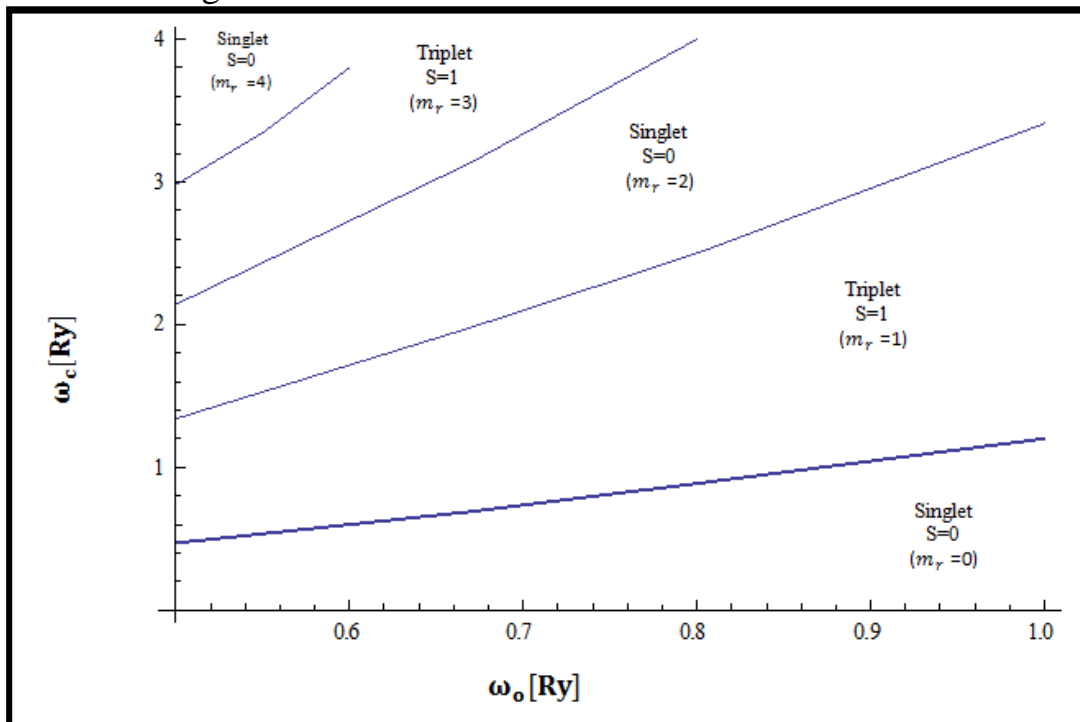


**Figure (3.3):** The singlet-triplet phase diagram of the quantum dot. The magnetic field strength  $\omega_c$  versus the confining frequency  $\omega_o$ .

This diagram shows the values of  $\omega_c$  at which the electron makes the singlet-triplet transition for specific value of  $\omega_0$ . It is also clear that as  $\omega_0$  increases the value of  $\omega_c$  needed to make the transition increases. For example the transition points are (0.6, 1.7, 2.7) and (0.88, 2.5, 4) for  $\omega_0$  0.6 and 0.8 respectively.

The exchange energy  $J$ , given in equation (2.14), for a particular confinement frequency ( $\omega_0 = \frac{2}{3}R^*$ ,  $0.5R^*$ ) had been plotted against the magnetic field strength ( $\omega_c$ ) as shown in figure 3.4(a) and figure 3.5, respectively. Figure 3.4(b) presents the exchange energy spectra for ( $\omega_0 = \frac{2}{3}R^*$ ) taken from Ref [44]. The two figures 3.4 (a and b) are plotted together in figure 3.4(c). From comparing both works very good agreement can be noticed.

These figures clearly show the crossing points ( $j=0$ ) at which the ground state angular momentum changes from singlet to triplet and vice versa at specific values of the magnetic field that depend on the confinement frequency. The numerical results for the exchange energy are presented in table 3.4.

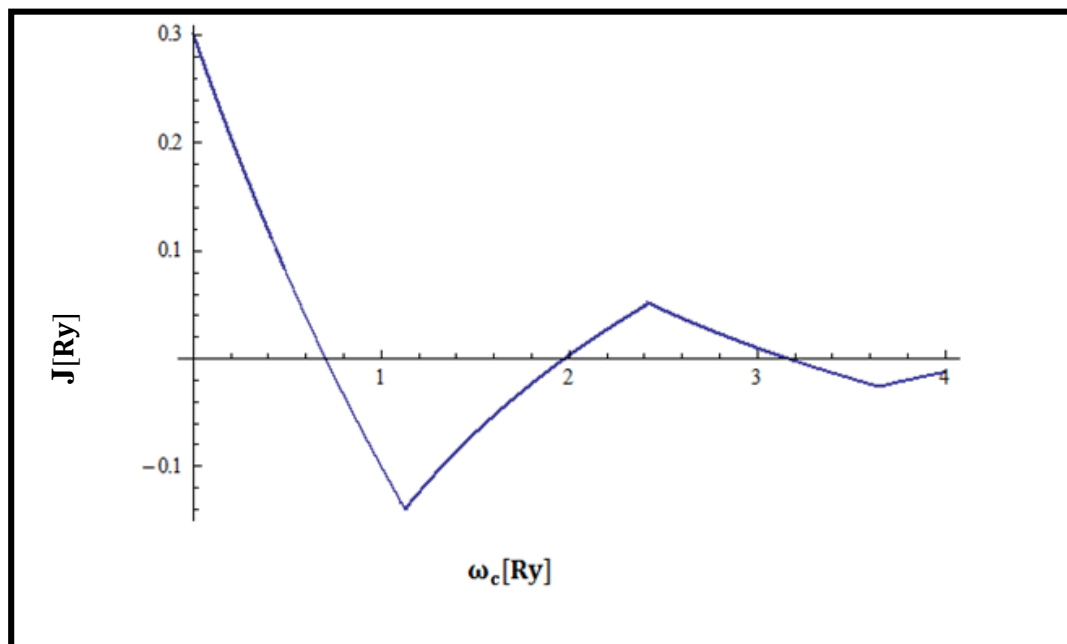


**Figure (3.4):** (a) The exchange energy of the QD versus the magnetic field strength for  $\omega_o = \frac{2}{3} R^*$ ,  $T = 0$  K,  $P = 0$  Kbar.

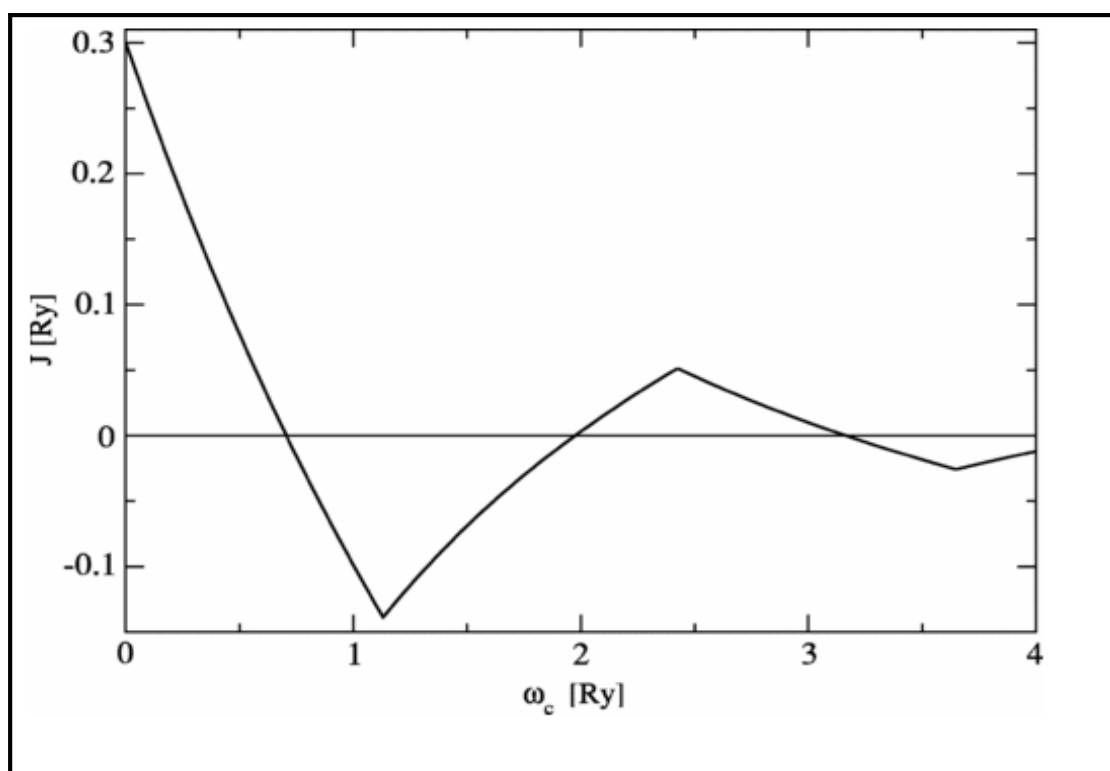


**Figure (3.4):** (b) The exchange energy of the QD versus the magnetic field strength for  $\omega_o = \frac{2}{3} R^*$ ,  $T = 0$  K,  $P = 0$  Kbar from Ref [44].

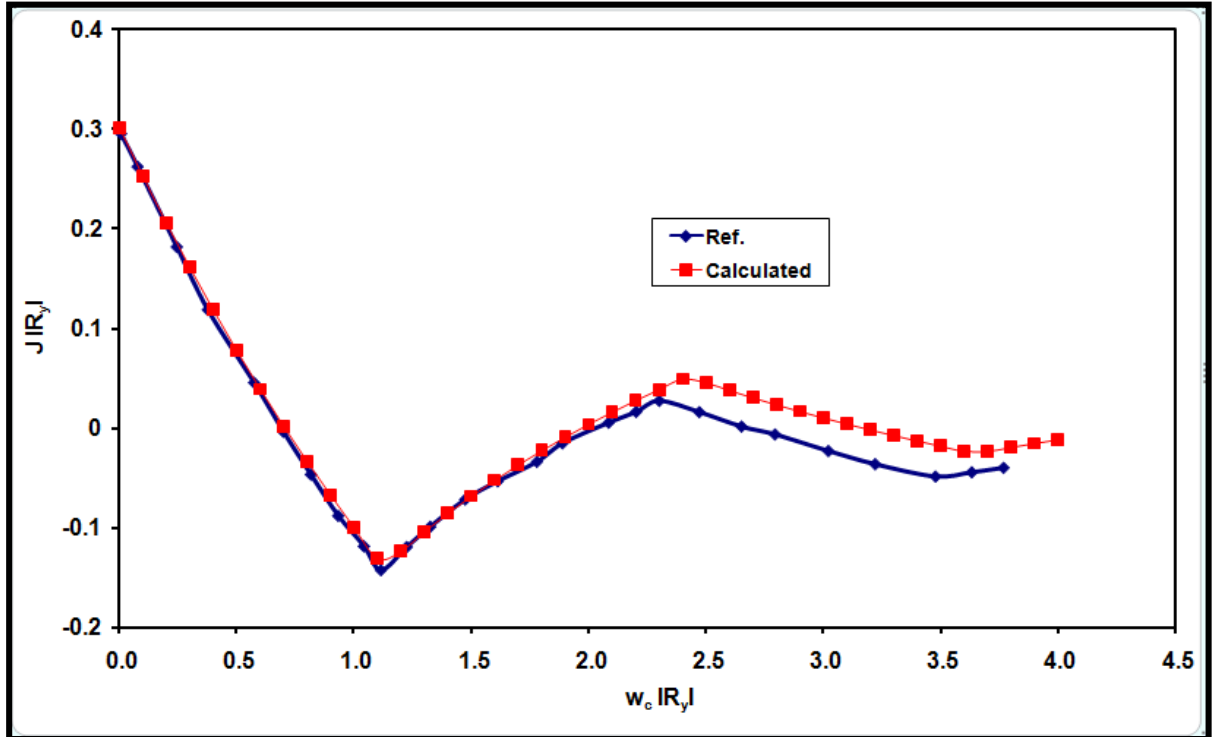


**Figure (3.4):** (c) The exchange energy of the QD versus the magnetic field strength for  $\omega_o = \frac{2}{3} R^*$ ,  $T = 0$  K,  $P = 0$  Kbar.

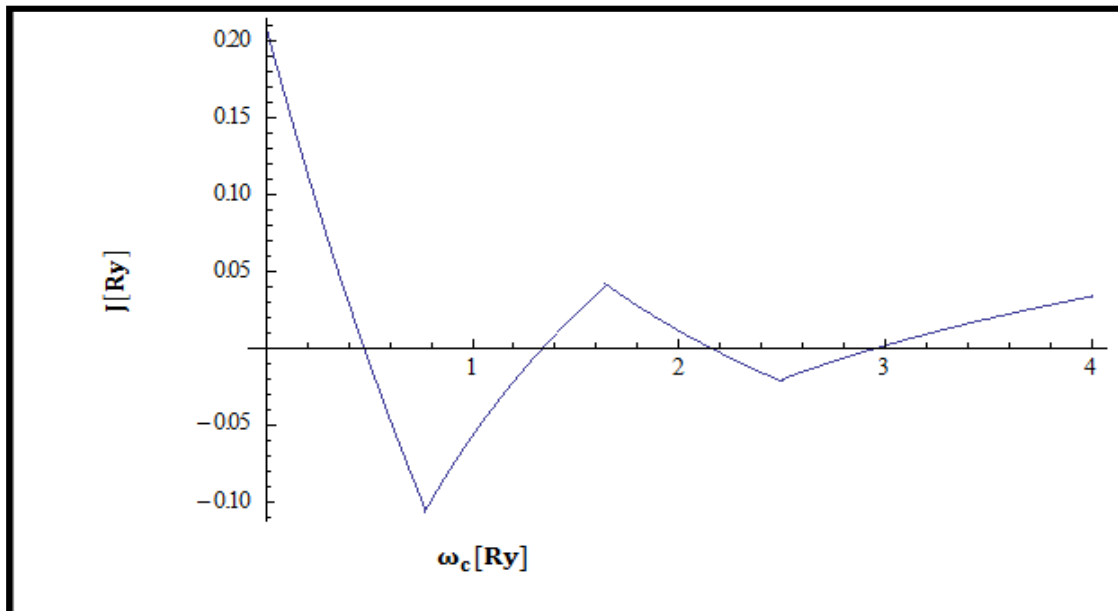


**Figure (3.5):** The exchange energy of the QD versus the magnetic field strength for  $\omega_o = 0.5 R^*$ ,  $T = 0$  K,  $P = 0$  Kbar.

**Table 3.4: The exchange energy of the quantum dot versus the strength of the magnetic field for  $\omega_o = \frac{2}{3} R^*$ ,  $T = 0$  K,  $P = 0$  Kbar.**

$\omega_c$ [Ry]	J [Ry]
0	0.301224
0.1	0.252303
0.2	0.205526
0.3	0.160853
0.4	0.118221
0.5	0.077545
0.6	0.038729
0.7	0.001665
0.8	-0.03376
0.9	-0.06766
1	-0.10014
1.1	-0.13131
1.2	-0.12395
1.3	-0.10428
1.4	-0.0859
1.5	-0.06869
1.6	-0.05253
1.7	-0.03732
1.8	-0.02298
1.9	-0.00942
2	0.003435
2.1	0.015641
2.2	0.027259
2.3	0.038338
2.4	0.048924
2.5	0.045305
2.6	0.037576
2.7	0.030219
2.8	0.023202
2.9	0.0165
3	0.010087
3.1	0.003941
3.2	-0.00196
3.3	-0.00762
3.4	-0.01308
3.5	-0.01833
3.6	-0.0234
3.7	-0.02368
3.8	-0.01964
3.9	-0.01574
4	-0.01198

To study the effect of the applied pressure and temperature on the energy spectra of the QD system, the dielectric constant as function of pressure and temperature has been plotted in Figures 3.6 and 3.7, while Figures 3.8 and 3.9 show the dependence of the effective mass parameter on the pressure and temperature. The figures clearly show that the dielectric constant decreases when the pressure rises and increases as the temperature rises, the figures also show that the effective mass enhances as the pressure rises and decreases as the temperature increases.

The energy of the QD is computed for three different pressures ( $P = 10$  Kbar,  $P = 20$  Kbar,  $P = 30$  Kbar) at fixed values of temperature and confining frequency ( $\omega_o = 0.5 R^*, T = 0K$ ). The computed energy results are plotted versus the magnetic field strength ( $\omega_c$ ) as in figures (3.10, 3.11, 3.12). The results show that the energy rises with enhancing hydrostatic pressure; this allows the assumption that the pressure makes larger electronic confinement in the structure. It also shows that the transition points remain unaffected in each case of increasing pressure.

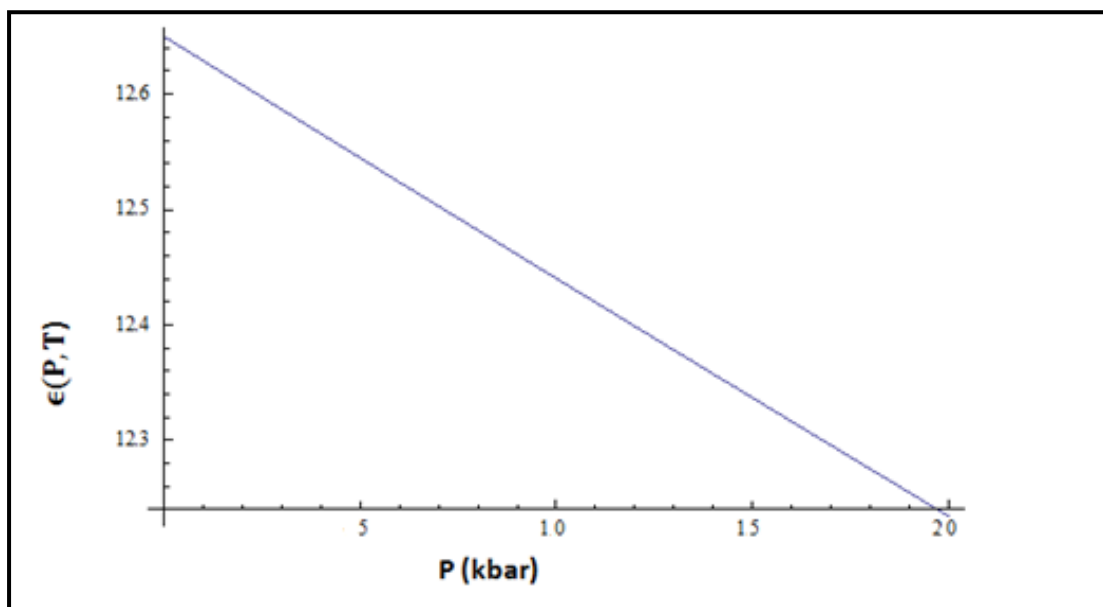


**Figure (3.6):** The pressure and temperature static dielectric constant against the hydrostatic pressure at  $T = 0$  K.

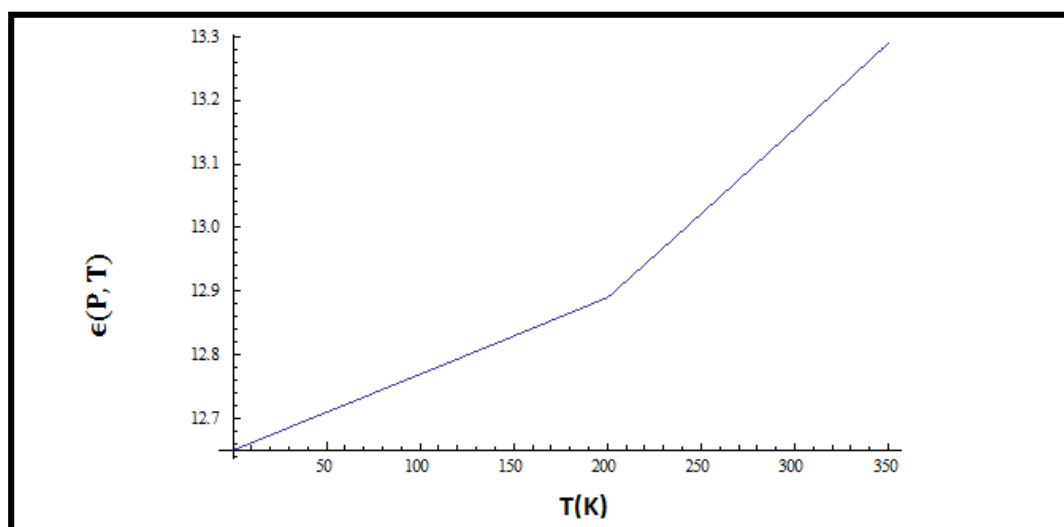


**Figure (3.7):** The pressure and temperature static dielectric constant against the temperature at  $P = 0$  Kbar.

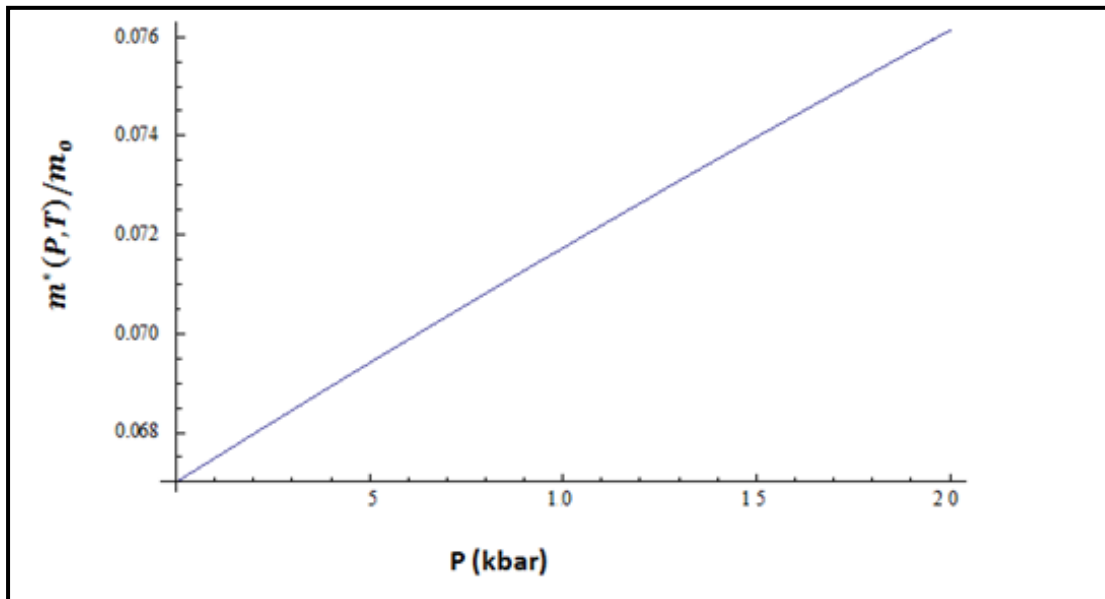


**Figure (3.8):** The pressure and temperature electron effective mass against the pressure at  $T = 0$  K.

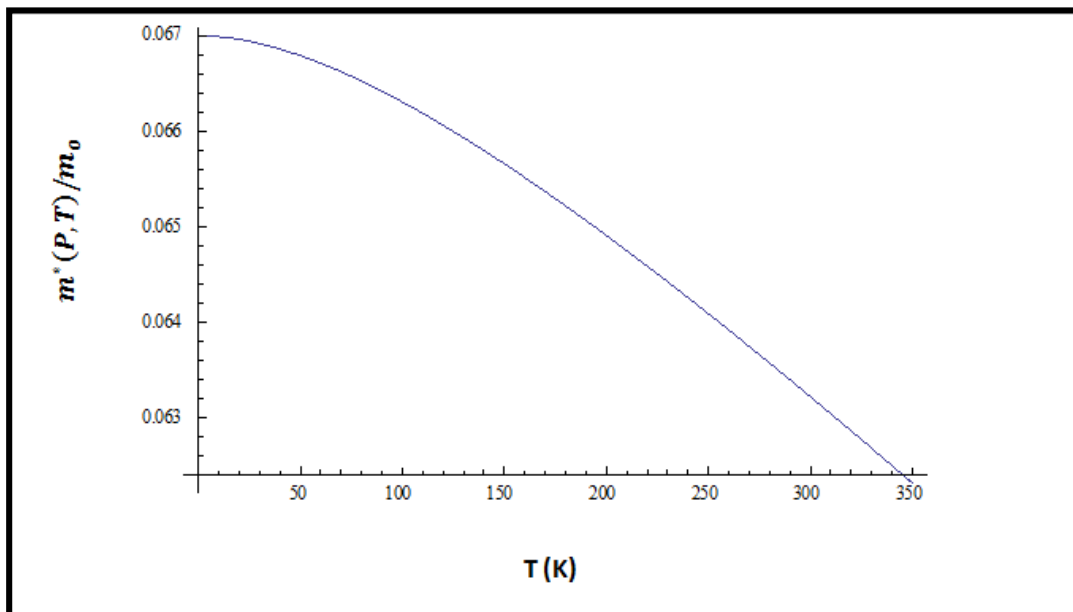


**Figure (3.9):** The pressure and temperature electron effective mass against the temperature at  $P = 0$  Kbar.



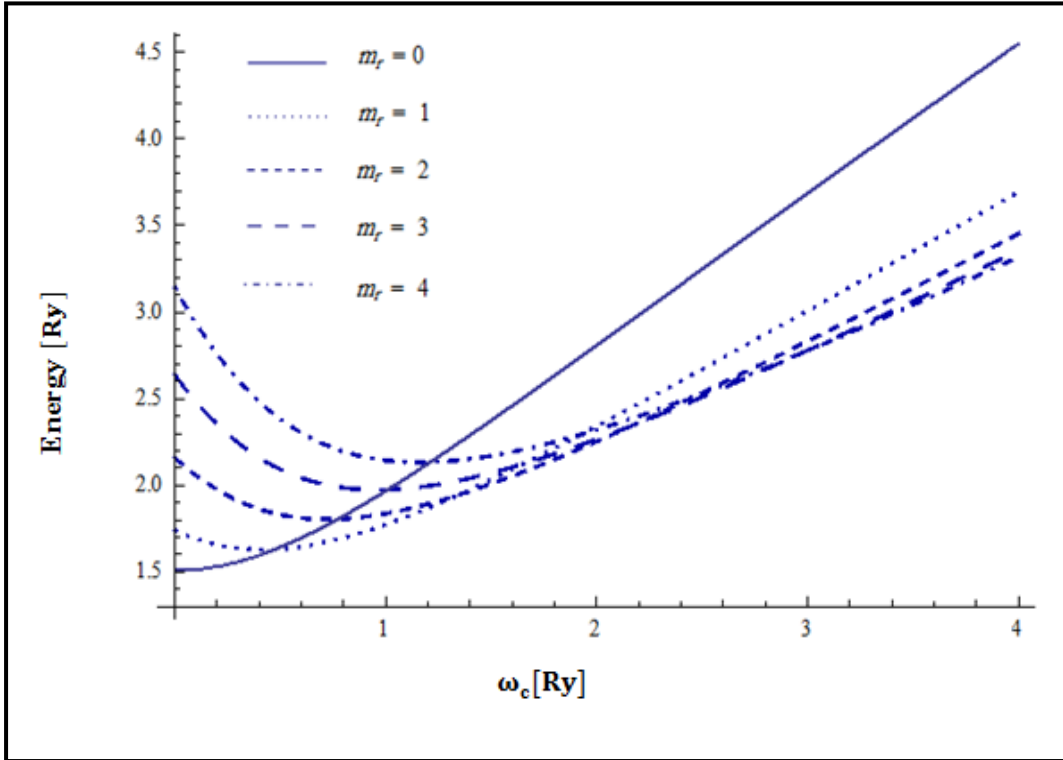


**Figure (3.10):** The computed energy spectra of quantum dot versus the strength of the magnetic field for  $\omega_0 = 0.5 R^*$ ,  $T = 0$  K,  $P = 10$  Kbar and angular momentum  $m_r = 0, 1, 2, 3, 4$ .

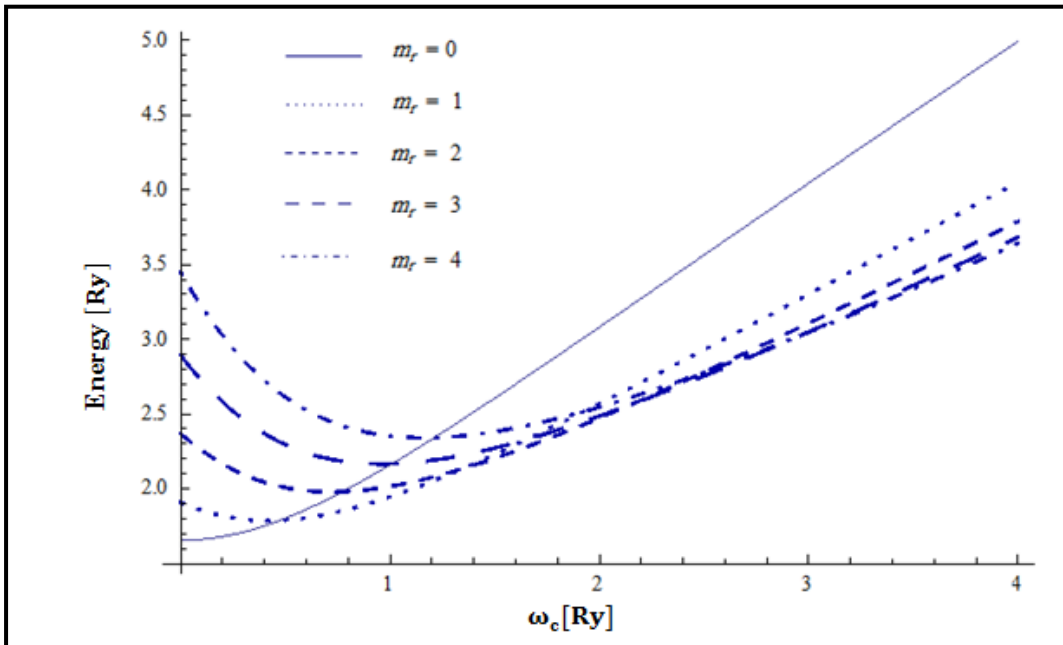


**Figure (3.11):** The computed energy spectra of quantum dot versus the strength of the magnetic field for  $\omega_0 = 0.5 R^*$ ,  $T = 0$  K,  $P = 20$  Kbar and angular momentum  $m_r = 0, 1, 2, 3, 4$ .

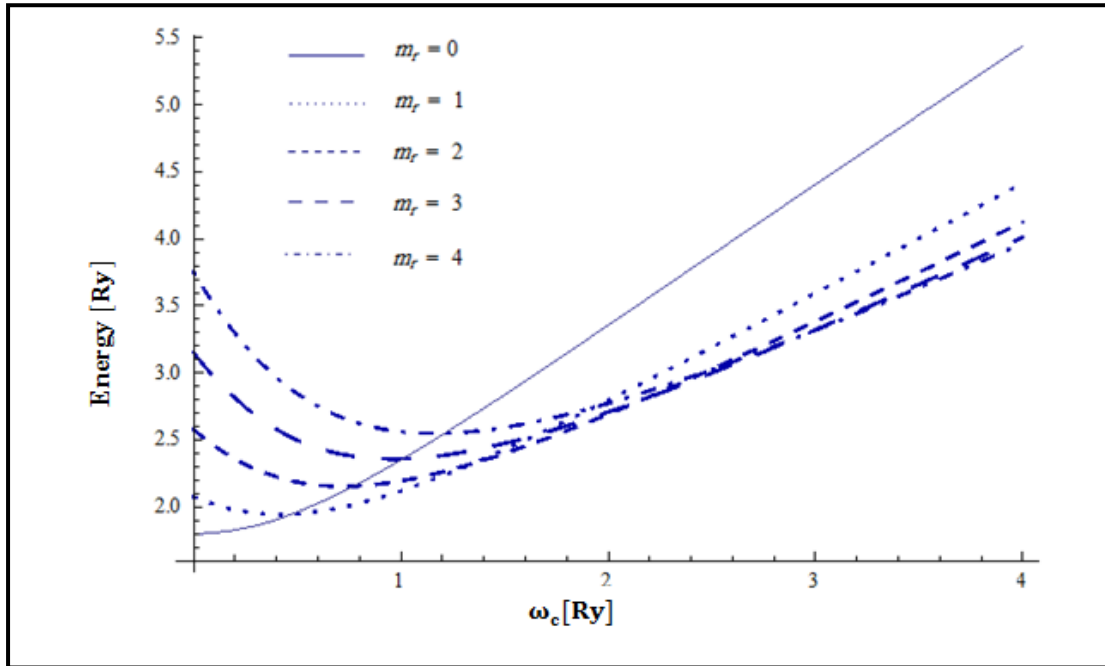


**Figure (3.12):** The computed energy spectra of quantum dot versus the strength of the magnetic field for  $\omega_0 = 0.5 R^*$ ,  $T = 0$  K,  $P = 30$  Kbar and angular momentum  $m_r = 0, 1, 2, 3, 4$ .

In order to show the effect of the pressure on the energy clearly, the ground state energy of the QD system ( $m = 0$ ) was plotted as a function of the magnetic field strength  $\omega_c$  for the four applied pressures ( $P = 0$  Kbar,  $P = 10$  Kbar,  $P = 20$  Kbar,  $P = 30$  Kbar). Figure 3.13 shows the upward shift in the ground state energy spectra which indicates that the energy increases as the pressure increases. This is due to the increase of the energy of the band-gap associated with decrease of the lattice parameter under pressure.

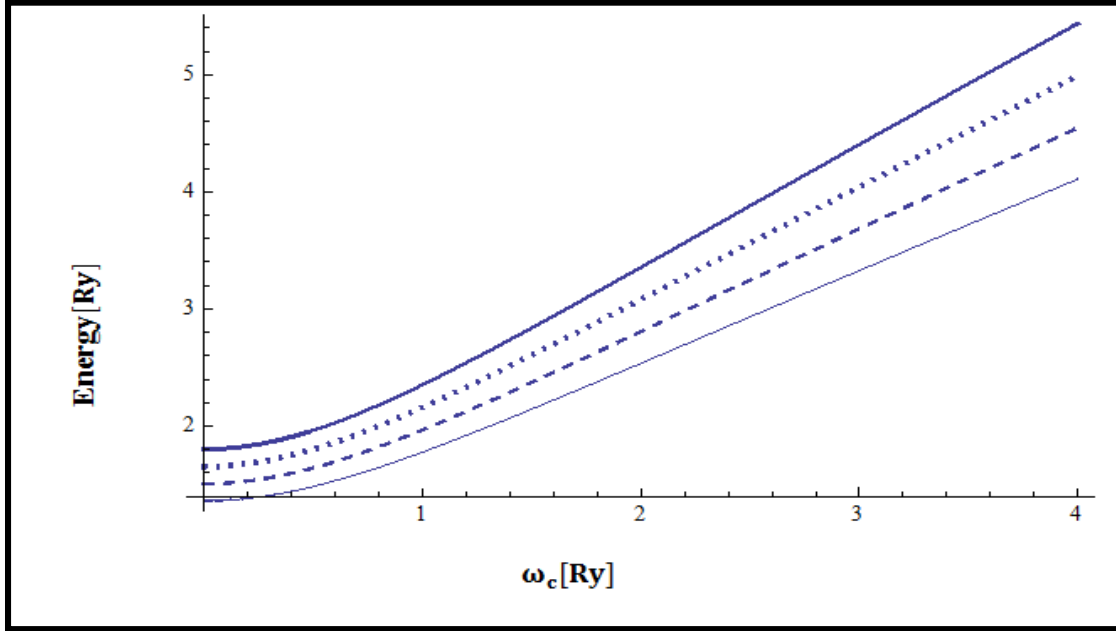


**Figure 3.13:** The computed energy spectra of quantum dot versus the strength of the magnetic field for  $\omega_0 = 0.5 R^*$ ,  $T=0$  K,  $m=0$  and various pressures ( $P = 0$  Kbar solid;  $P = 10$  Kbar dashed;  $P = 20$  Kbar dotted and  $P = 30$  Kbar thick).

This energy-pressure behavior can be understood from the effective mass and dielectric constant pressure-temperature relations plotted in figures 3.6 and 3.8. As the pressure increases the dielectric constant decreases for zero temperature and this leads to an enhancement in the electron – electron coulomb interaction in the QD-Hamiltonian. However, the effective mass increases and thus the kinetic energy term decreases. This coulomb energy and kinetic energy behavior terms lead to an effective increase in the energy levels of the QD spectra.

Figures (3.14, 3.15, 3.16, 3.17) shows the variation of the exchange energy versus the strength of the magnetic field ( $\omega_c$ ) for the three applied pressures ( $P = 10$  Kbar,  $P = 20$  Kbar,  $P = 30$  Kbar). As seen in these figures, an increase in the hydrostatic pressure raises the exchange energy spectra of the QD system without affecting the angular momentum transition points.

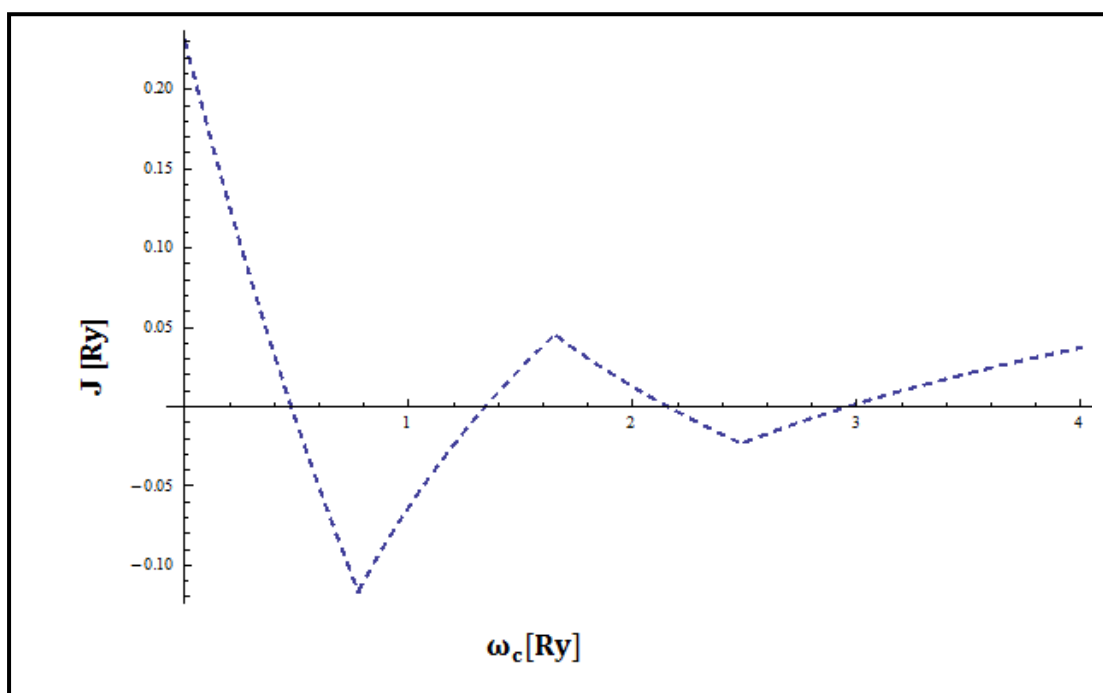


**Figure (3.14):** The exchange energy of the QD system versus the magnetic field strength for  $\omega_o = 0.5 R^*$ ,  $T = 0$  K,  $P = 10$  Kbar.

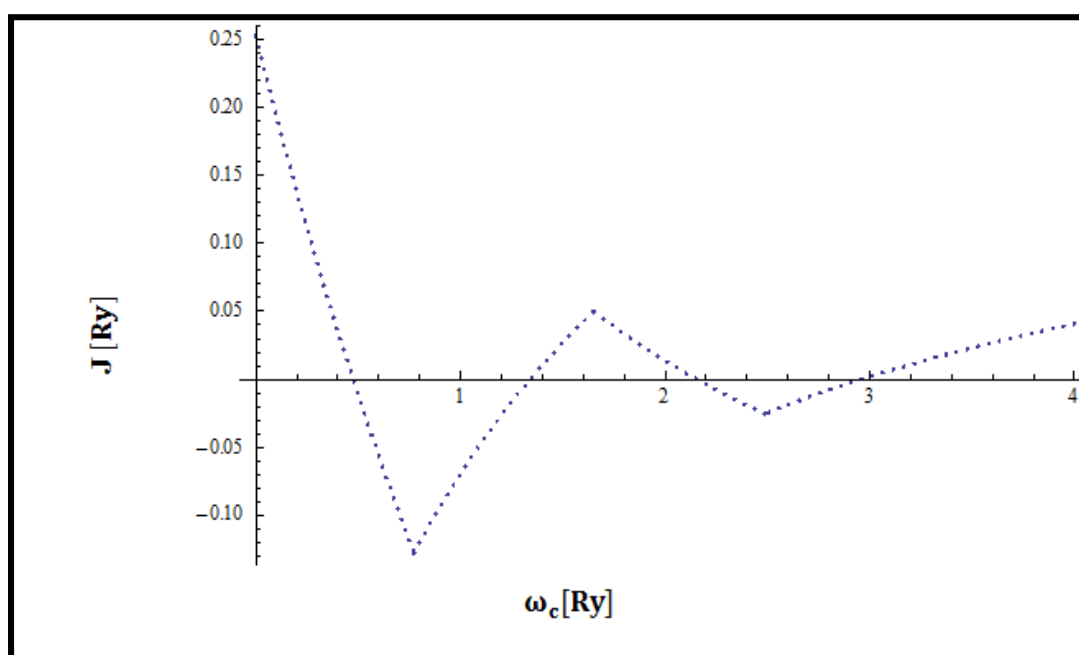


**Figure (3.15):** The exchange energy of the QD system versus the magnetic field strength for  $\omega_o = 0.5 R^*$ ,  $T = 0$  K,  $P = 20$  Kbar.

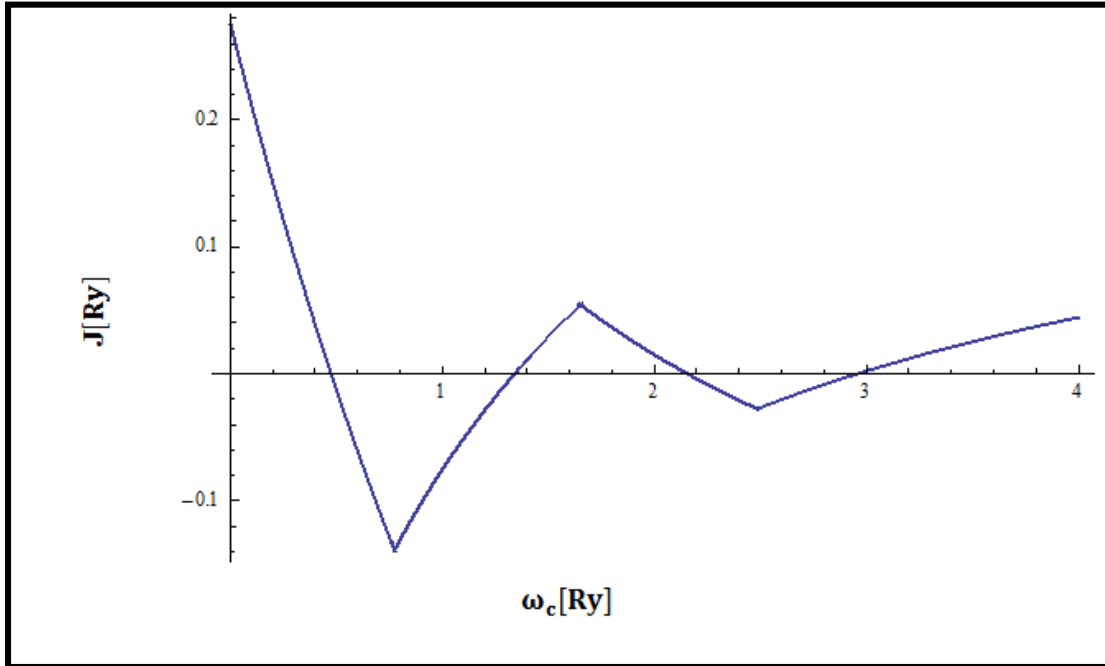


**Figure (3.16):** The exchange energy of the QD system versus the magnetic field strength for  $\omega_o = 0.5 R^*$ ,  $T = 0$  K,  $P = 30$  Kbar.

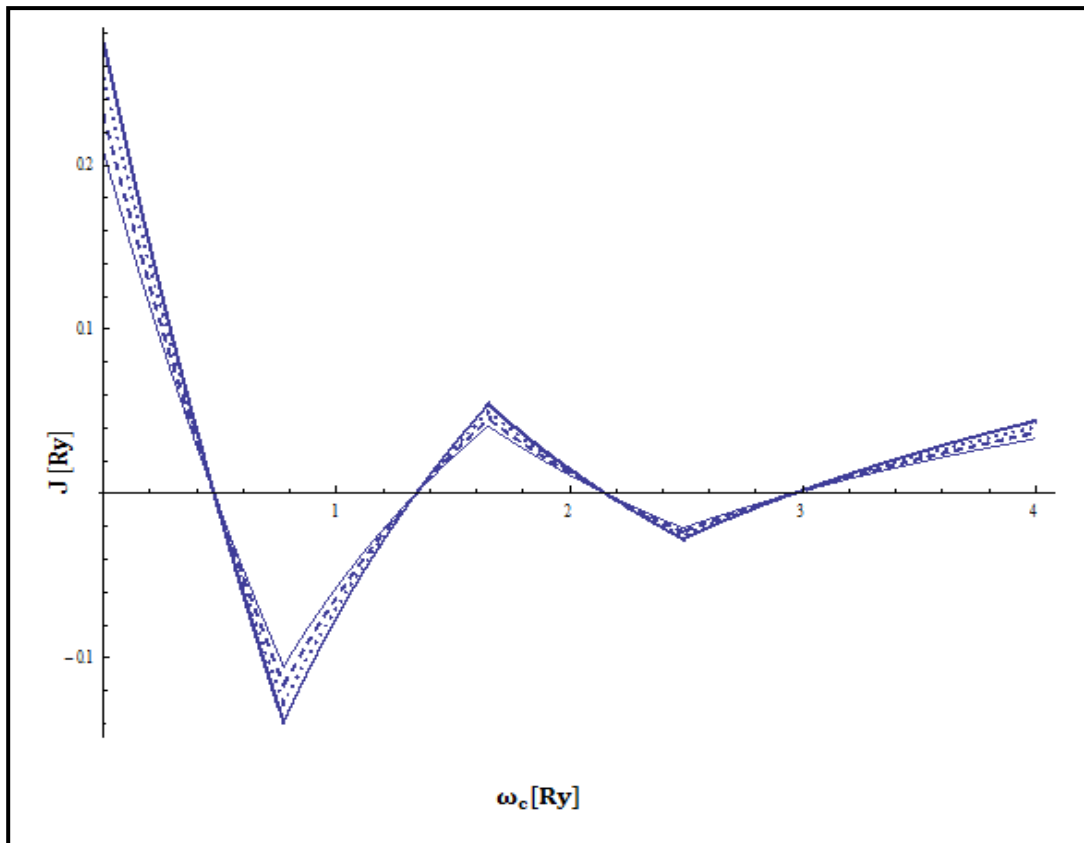


**Figure (3.17):** The exchange energy of the QD system versus the magnetic field strength for  $\omega_o = 0.5 R^*$ ,  $T = 0$  K and various pressures ( $P = 0$  Kbar solid;  $P = 10$  Kbar dashed,  $P = 20$  Kbar dotted and  $P = 30$  Kbar thick).

To study the effect of the temperature on the energy spectra of the QD system, the energy is computed for three different temperatures ( $T = 0$  K,  $T = 150$  K,  $T = 350$  K) at fixed values of external pressure and confining frequency ( $\omega_0 = 0.5 R^*$ ,  $P = 0$  Kbar). The computed energy results are plotted against the strength of the magnetic field ( $\omega_c$ ) as in figures (3.18, 3.19). The results show that the energy decreases as the temperature increases. It also shows that the transition points remain unaffected in each case of increasing Temperature.

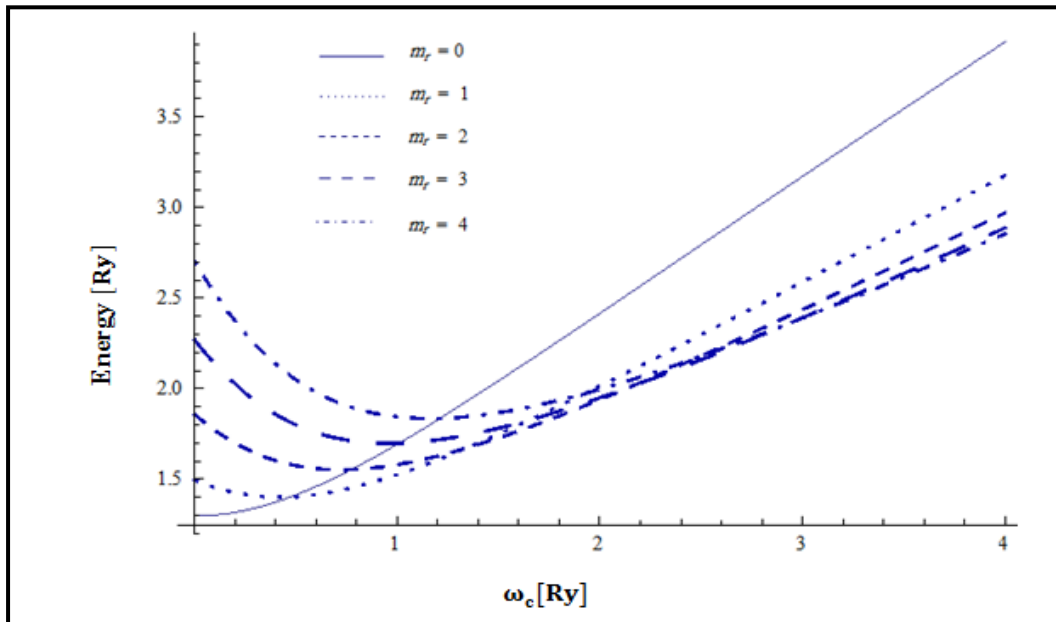


**Figure (3.18):** The energy of the quantum dot system versus the magnetic field strength for  $\omega_0 = 0.5 R^*$ ,  $T = 150$  K,  $P = 0$  Kbar and angular momentum  $m_r = 0, 1, 2, 3, 4$ .

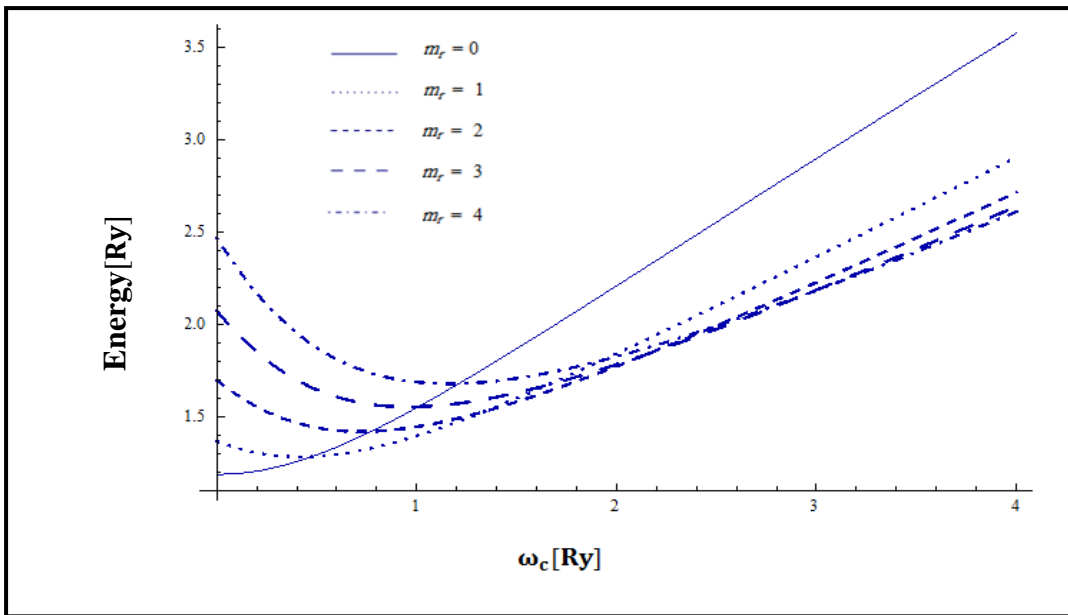


**Figure (3.19):** The energy of the quantum dot system versus the magnetic field strength for  $\omega_0 = 0.5 R^*$ ,  $T = 350$  K,  $P = 0$  Kbar and angular momentum  $m_r = 0, 1, 2, 3, 4$ .

To show the effect of the temperature on the energy clearly, the ground state energy of the quantum dot system ( $m_r = 0$ ) was plotted against the magnetic field strength  $\omega_c$  for the three applied different temperatures ( $T = 0$  K,  $T = 150$  K,  $T = 350$  K). In figure 3.20, it can be seen that there is a shift downwards in the ground state energy spectra which indicates that the energy decreases as the temperature increases.

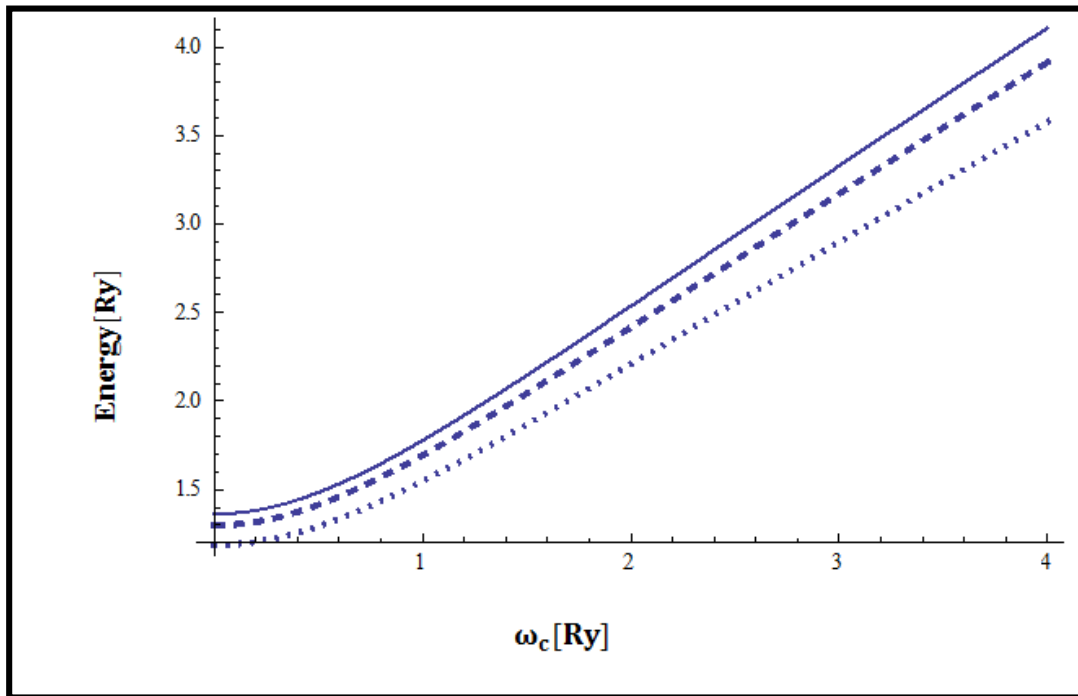


**Figure (3.20):** The energy of the quantum dot system versus the magnetic field strength for  $\omega_0 = 0.5 R^*$ ,  $P = 0$  Kbar,  $m = 0$  and various temperatures ( $T = 0$  K solid,  $T = 150$  K dashed and  $T = 350$  K dotted).

This behavior can be explained according to figure 3.7 and figure 3.9. It is noticed that as the temperature increases, the dielectric constant increases and the effective mass decreases which results in a decrease in the coulomb and confinement energy and an increase in the kinetic energy. This leads to an effective decrease in the energy levels of the QD spectra.

Figures (3.21, 3.22, 3.23) shows the variation of the exchange energy versus the strength of the magnetic field ( $\omega_c$ ) for the three applied temperatures ( $T = 0$  K,  $T = 150$  K,  $T = 350$  K). As seen in these figures, an increase in the temperature decreases the exchange energy spectra in a



small amount but leaves the transition points unaffected due to the increases of the system entropy.

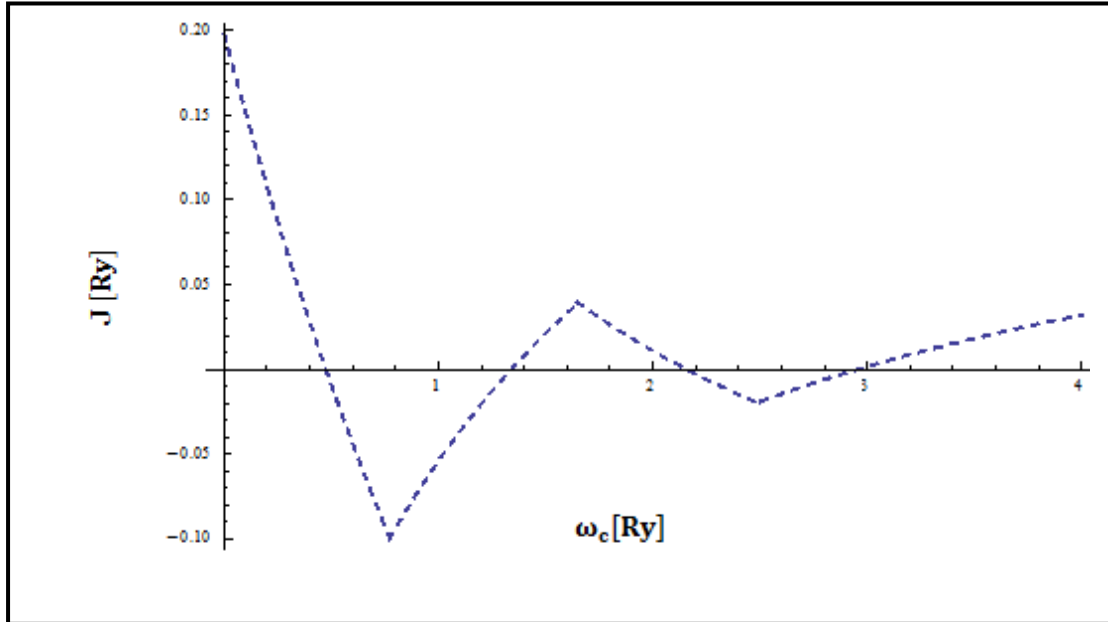


**Figure (3.21):** The exchange energy of the QD system versus the magnetic field strength for  $\omega_o = 0.5 R^*$ ,  $T = 150$  K,  $P = 0$  Kbar.

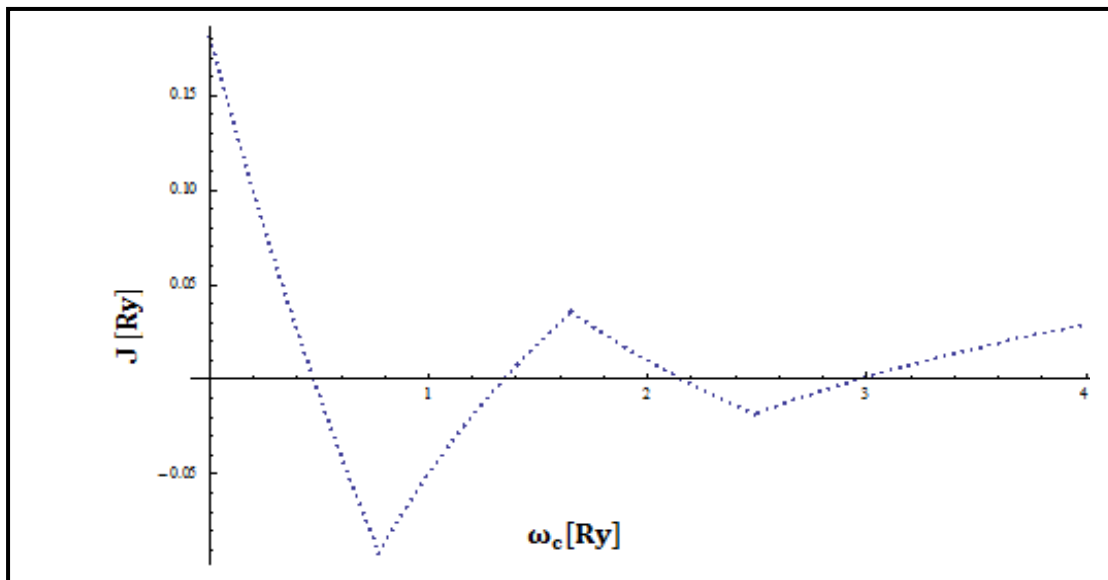


**Figure (3.22):** The exchange energy of the QD system versus the magnetic field strength for  $\omega_o = 0.5 R^*$ ,  $T = 350$  K,  $P = 0$  Kbar.

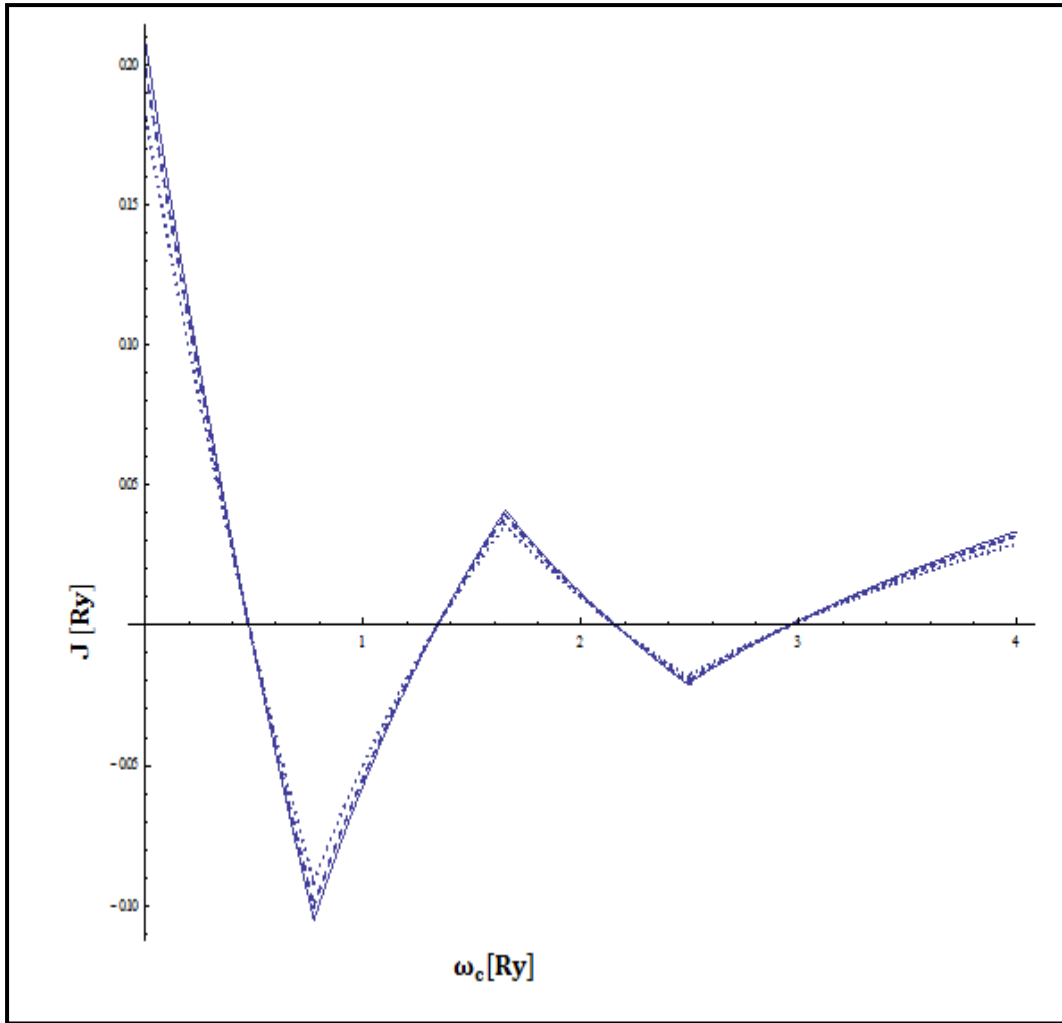


**Figure (3.23):** The exchange energy of the QD system versus the magnetic field strength for  $\omega_o = 0.5 R^*$ ,  $P = 0$  Kbar and various temperatures ( $T = 0$  K solid;  $T = 150$  K dashed  $T = 350$  K dotted).

Finally, to clarify the above results the dependence of the energy on the hydrostatic pressure for three different temperatures ( $T = 0$  K,  $T = 150$  K,  $T = 350$  K) at fixed values of confining frequency and magnetic field strength ( $\omega_o = 0.5 R^*$ ,  $\omega_c = 0R^*$ ) was studied and the results are presented in figure 3.24. It is noticed that the energy rises with enhancing pressure which agrees with the results in figure 3.13.

The variation of the energy with respect to the hydrostatic pressure and temp

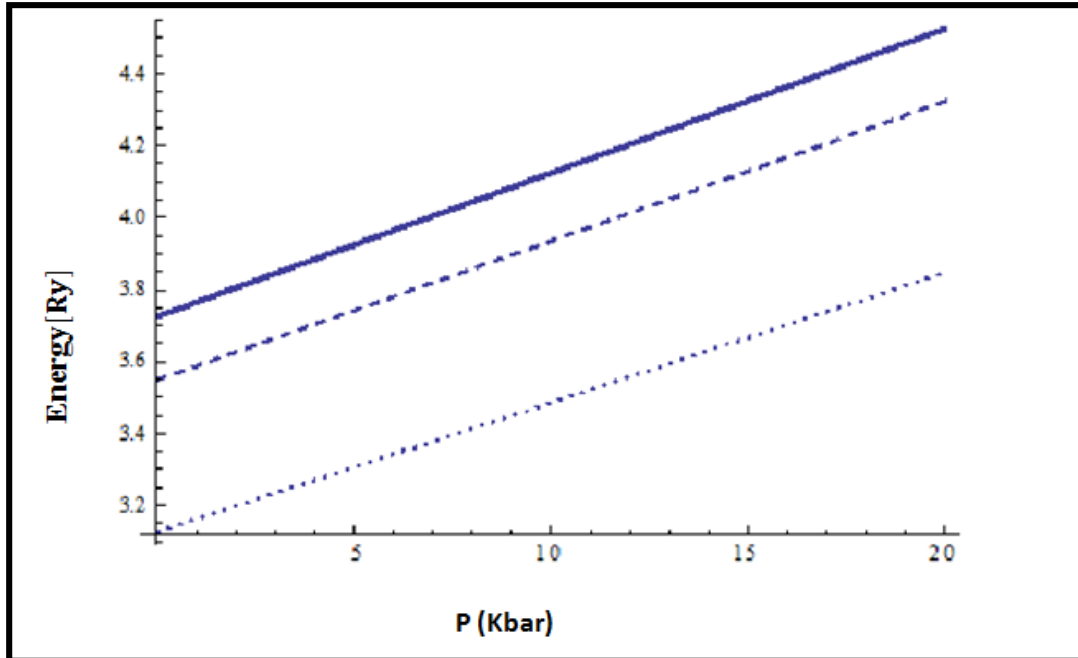


**Figure (3.24):** The energy of the QD system against the hydrostatic pressure for  $\omega_o = 0.5 R^*$ ,  $\omega_c = 0 R^*$ ,  $m_r = 0$  and various temperatures (T = 0 K solid; T = 150 K dashed; T = 350 K dotted).

The energy dependence on the temperature for four different pressures (P = 0 Kbar, P = 2 Kbar, P = 5 Kbar, P = 7 Kbar) at fixed values of confining frequency and magnetic field strength ( $\omega_o = 0.5 R^*$ ,  $\omega_c = 0 R^*$ ) was also studied and results are presented in figure 3.25. It is seen that the energy reduces as the temperature increases which agrees with the results in figure 3.20

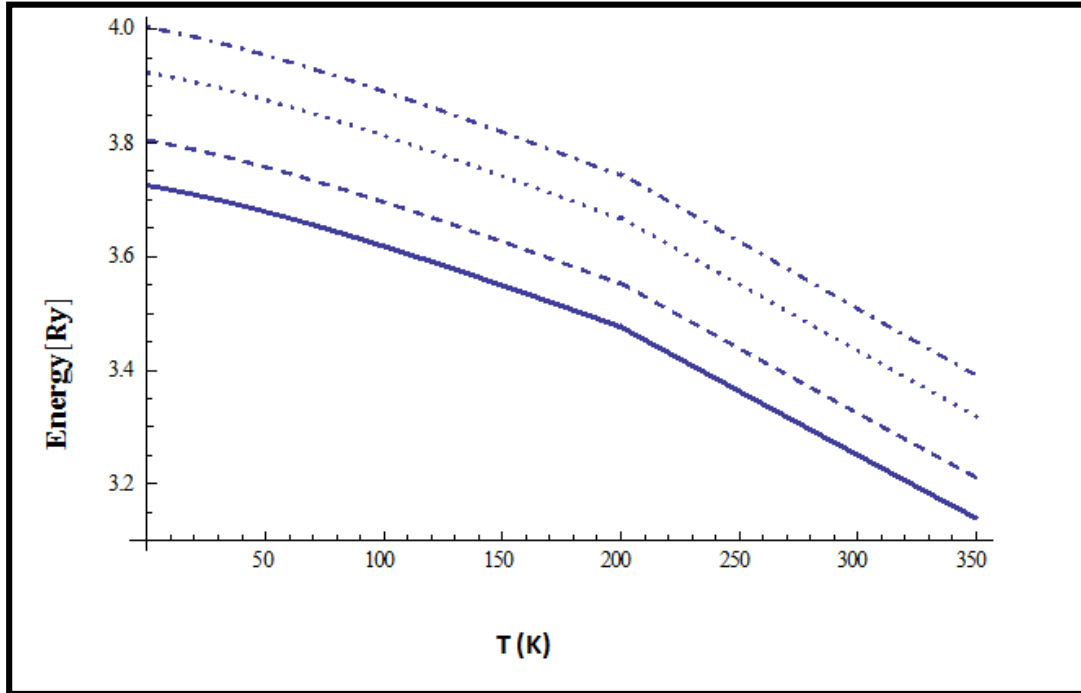


**Figure (3.25):** The energy of the QD system against the temperature for  $\omega_o = 0.5 R^*$ ,  $\omega_c = 0 R^*$  and various pressures (P = 0 Kbar solid; P = 2 Kbar dashed; P = 5 Kbar dotted and P = 7 Kbar dash-dotted).

In all steps of calculations, the issue of convergence had been insured. In Figure 3.26, the energy was plotted against the number of basis ( $s_p$ ) for ( $\omega_o = 0.5 R^*$ ,  $\omega_c = 1 R^*$ ,  $m = 2$ ). The figure clearly shows the numerical stability of the energy as the number of basis is increased. For example the energies had been converged to  $E = 1.65948$  Ry, 1.65942 Ry, 1.65941 Ry and 1.65941 Ry for basis numbers  $s_p = 5, 10, 20$  and 30, respectively. Figure 3.27 shows the convergence for ( $\omega_o = 0.5 R^*$ ,  $\omega_c = 5 R^*$ ,  $m = 2$ ).

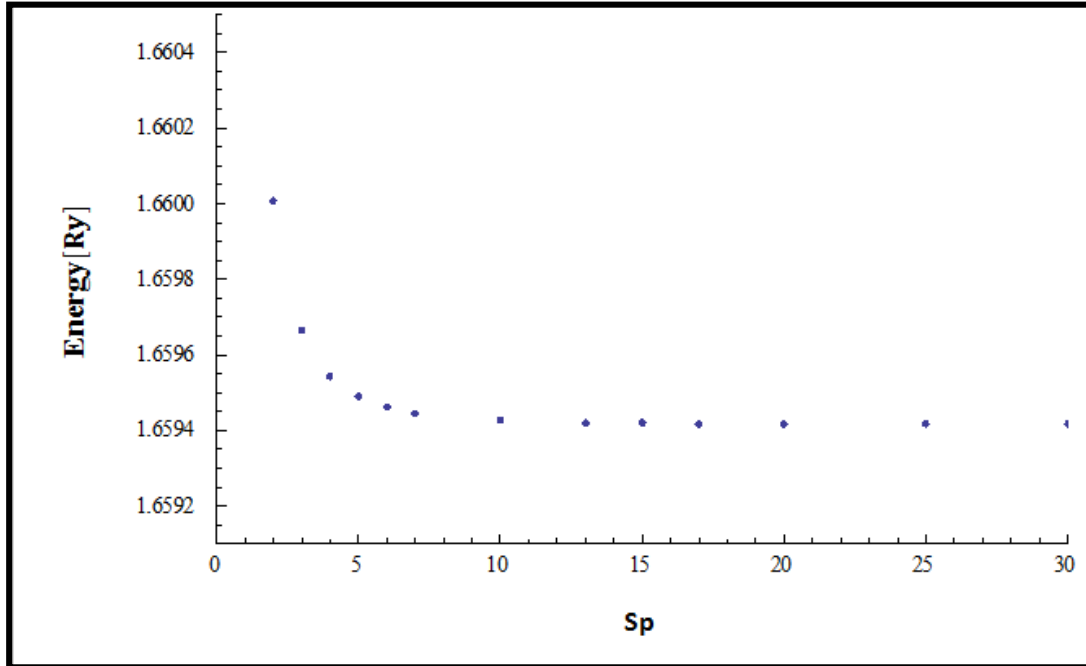


**Figure (3.26):** The computed energy of a two electron quantum dot for  $m = 2$ ,  $\omega_c = 1 R^*$  and  $\omega_0 = 0.5 R^*$ , against the number of basis ( $s_p$ ) taken in diagonalization process.

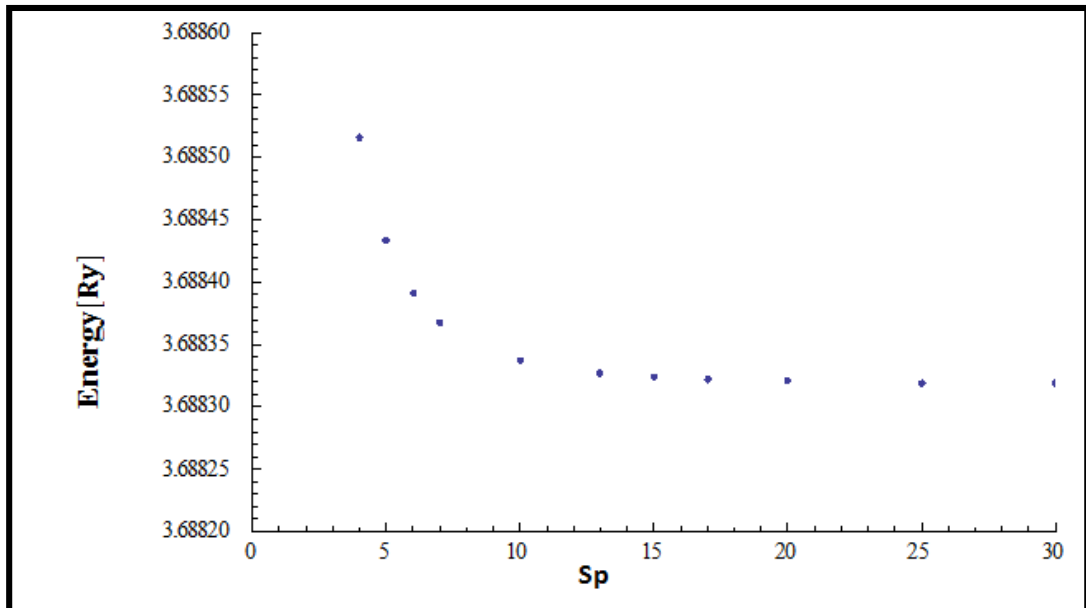


**Figure (3.27):** The computed energy of a two electron quantum dot for  $m = 2$ ,  $\omega_c = 5 R^*$  and  $\omega_0 = 0.5 R^*$ , against the number of basis ( $s_p$ ) taken in diagonalization process.

## Chapter four

### Conclusion

The Hamiltonian for a parabolic GaAs quantum dot presented in a magnetic field had been solved by applying exact diagonalization method. The Fock-Darwin states had been used as basis to evaluate the coulomb matrix element and to give the result in a closed form. In addition, the transitions of angular momentum in the ground state of GaAs quantum dot spectra had been shown. These transitions are related to the coulomb interaction and correspond to the (singlet-triplet) transitions. The comparison shows that our results are in very good agreement with the reported works.

Using the effective mass approximation, the binding energy dependence on both the temperature and hydrostatic pressure corresponding to the ground state of GaAs/AlGaAs quantum dot had been investigated. The investigations had shown clearly that increasing the applied hydrostatic pressure enhances the binding energy while enhancing the temperature decreases the binding energy. The results of this work show that effects of the applied pressure and temperature on the binding energy of GaAs/AlGaAs quantum dot should be considered.

These quantum dots can be used in a variety of applications such as spin-based quantum computer.

In this work, the effect of the applied pressure, temperature and magnetic field on the energy states of a single quantum dot had been taken. In the

future, magnetic properties like magnetization and magnetic susceptibility, thermodynamic properties like heat capacity can be investigated. Also, the properties of two or more electrons quantum dot are possible to study.

## References

- [1] A. *Coronado*, *EEE-5425*, 2605672 (2013).
- [2] P. Harrison, *Quantum Wells, Wires and Dots*, John Wiley & Sons, 2<sup>nd</sup> edition, 243 (2015).
- [3] O. Ciftja and A. Anil Kumar, *Phys. Rev.* **B 70**, 205326 (2004).
- [4] B. Boyacioglu and A. Chatterjee, *J. Appl. Phys.* **112**, 083514 (2012).
- [5] D. Loss and D. P. Divincenzo, *Phys. Rev.* **A 57**, 120 (1998).
- [6] G. Burkard, D. Loss and D. P. Divincenzo, *Phys. Rev.* **B 59**, 2070 (1999).
- [7] R. C. Ashoori, H. L. Stormer, J. S. Weiner, L. N. Pfeiffer, K. W. Baldwin, and K. W. West., *Phys. Rev. Lett.* **71**, 613 (1993).
- [8] R. C. Ashoori, *Nature* **379**, 413 (1996)
- [9] O. Ciftja, *Phys. Scr.* **88**, 058302 (2013).
- [10] M. A. Kastner, *Rev. Mod. Phys.* **64**, 849 (1992).
- [11] M. Henini, *Nanoscale Res. Lett.* **1**, 32–45 (2006)
- [12] CA. Dai, YL. Wu, YH. Lee, CJ. Chang, WF. Su, *J. Cryst. Growth*, **288**, 128–136 (2006).
- [13] J. Schwarz, C. Contescu, K. Putyera, *Dekker Encyclopedia of Nanoscience and Nanotechnology*, CRC Press, **4** (2004).
- [14] D. Bodas, C. Khan-Malek, *Sens. Actuator B-Chem.*, **128**, 168–172 (2007).
- [15] Q. Ma, TY. Song, P. Yuan, C. Wang, XG .Su, *Colloid Surf. B-Biointerfaces.* **64**:248–254 (2008).
- [16] A. Rastelli et al., *PhysRevLett.* **92**, 166104 (2004).



- [17] L. Kouwenhoven, C. Marcus, *Physics World*, **11**, 35-39 (1998).
- [18] J. Q. You, Franco Nori, *Nature*, **474**, 589–597 (2011).
- [19] Et viola, m.brooks, *new scientist*, 2149, 22-25(1998).
- [20] M. Taut, *J. Phys. A* **27**, 1045 (1994).
- [21] B. S. Kandemir, *Phys. Rev. B* **72**, 165350 (2005).
- [22] P. A. Maksym and T. Chakraborty, *Phys. Rev. Lett.* **65**, 108 (1990).
- [23] M. El-said, *Turkish J. Physics*, **26**, 1 (2002).
- [24] M. El-said, *Semiconductor science and technology*, **10**, 1310 (1995).
- [25] M. El-Said, *Journal de Physique I*, **5**, 1027-1036 (1995).
- [26] M. El-said, *Physica Scripta*, **75** , 436 (2007).
- [27] M. El-said, *Chinese Journal of Physics*, **40**, 315-324 (2002).
- [28] M. El-said, M. Al-Naafa, S. Zugail, *Journal of Computational and Theoretical Nanoscience*, **5**, 677-680 (2008).
- [29] M. El-said, M. AL-Naafa, S. Zugail, *Indian Journal of Pure and Applied Physics*, **46**, 876 (2008).
- [30] P. A. Maksym, *Phys. Rev. B* **53**, 10 871 (1996).
- [31] F. Bolton, *Phys. Rev. B* **54**, 4780 (1996).
- [32] J. Kainz, S. A. Mikhailov, A. Wensauer, and U. Rössler, *Phys. Rev. B* **65**, 115305 (2002).
- [33] M. Koskinen, M. Manninen, and S. M. Reimann, *Phys. Rev. Lett.* **79**, 1389 (1997).
- [34] K. Hirose and N. S. Wingreen, *Phys. Rev. B* **59**, 4604 (1999).
- [35] De Groote JJ, Hornos JE, Chaplik AV, *Phys Rev B* **19**, 12773-12776 (1992).

- [36] N.T.T.Nguyen, F.M.Peeters, Phys. Rev. **B 78**, 045321(2008).
- [37] M.Helle, A. Harju, R.M.Nieminen, Phys. Rev. **B 72**, 205329(2005).
- [38] G. Rezaei, S. Shojaeian Kish, Physica E: Low-dimensional Systems and Nanostructures, **45**, 56-60 (2012).
- [39] G. Rezaei, S.F. Taghizadeh, A.A. Enshaeian, Physica **E 44** , 1562, (2012).
- [40] M. Kirak, Y. Altinok, S. Yilmaz, Journal of Luminescence **136**,415–421(2013).
- [41] Y.Wen, M.Yang, S.J.Xu, L.Qin and ZX.Shen, Journal of applied physics **112**, 014301 (2012)
- [42] A. Sivakami, M. Mahendran, Physica **B 405**,1403-1407 (2010).
- [43] N.T.T.Nguyen, S. Das Sarma, Phys. Rev. **B 83**, 235322-235345 (2011).
- [44] W.Dybalski, P.Hawrylak, Phys. Rev. **B 72**, 205432-205441(2005).

## Appendix

### Appendix A: decoupling of the quantum dot Hamiltonian into center of mass ( $R$ ) and relative ( $r$ ) parts.

The Hamiltonian can be explicitly expressed in terms of coordinates and momenta as follows:

$$\hat{H} = \frac{1}{2}m r_1^2 \omega_o^2 + \frac{1}{2}m r_2^2 \omega_o^2 + \frac{e^2}{\epsilon|\mathbf{r}_2 - \mathbf{r}_1|} + \frac{\left(\mathbf{p}_1 + \frac{e \mathbf{A}(\mathbf{r}_1)}{c}\right)^2}{2m} + \frac{\left(\mathbf{p}_2 + \frac{e \mathbf{A}(\mathbf{r}_2)}{c}\right)^2}{2m} \quad (\text{A.1})$$

By using the standard coordinate transformation, the quantum dot Hamiltonian can be decoupled into center of mass ( $R$ ) and relative ( $r$ ) parts.

$$\mathbf{R} = \frac{\mathbf{r}_1 + \mathbf{r}_2}{2} \quad (\text{A.2})$$

$$\mathbf{r} = \mathbf{r}_2 - \mathbf{r}_1 \quad (\text{A.3})$$

$$\mathbf{P}_R = \mathbf{p}_1 + \mathbf{p}_2 \quad (\text{A.4})$$

$$\mathbf{p}_r = \frac{\mathbf{p}_2 - \mathbf{p}_1}{2} \quad (\text{A.5})$$

So the Hamiltonian can be written as,

$$\hat{H} = \frac{\left(\frac{e \mathbf{A}\left(-\frac{\mathbf{r}}{2} + \mathbf{R}\right)}{c} - \mathbf{p}_r + \frac{\mathbf{P}_R}{2}\right)^2}{2m} + \frac{\left(\frac{e \mathbf{A}\left(\frac{\mathbf{r}}{2} + \mathbf{R}\right)}{c} + \mathbf{p}_r + \frac{\mathbf{P}_R}{2}\right)^2}{2m} + \frac{1}{2}m\left(-\frac{\mathbf{r}}{2} + \mathbf{R}\right)^2 \omega_o^2 + \frac{1}{2}m\left(\frac{\mathbf{r}}{2} + \mathbf{R}\right)^2 \omega_o^2 + \frac{e^2}{\epsilon r} \quad (\text{A.6})$$

Confining potential terms can be expressed as:

$$\frac{1}{2}m\left(-\frac{\mathbf{r}}{2} + \mathbf{R}\right)^2 \omega_o^2 + \frac{1}{2}m\left(\frac{\mathbf{r}}{2} + \mathbf{R}\right)^2 \omega_o^2 = \frac{1}{4}m r^2 \omega_o^2 + m R^2 \omega_o^2 \quad (\text{A.7})$$

Using the linear property of the vector potential, we can separate kinetic energy terms into center of mass and relative part:

$$\begin{aligned}
& \frac{\left( \frac{e \mathbf{A} \left( -\frac{\mathbf{r}}{2} + \mathbf{R} \right)}{c} - \mathbf{p}_r + \frac{\mathbf{P}_R}{2} \right)^2}{2m} + \frac{\left( \frac{e \mathbf{A} \left( \frac{\mathbf{r}}{2} + \mathbf{R} \right)}{c} + \mathbf{p}_r + \frac{\mathbf{P}_R}{2} \right)^2}{2m} \\
& = \frac{\left( \frac{e \mathbf{A}(\mathbf{r})}{2c} + \mathbf{p}_r \right)^2}{m} + \frac{\left( \frac{2e \mathbf{A}(\mathbf{R})}{c} + \mathbf{P}_R \right)^2}{4m}
\end{aligned} \tag{A.8}$$

The full QD Hamiltonian in  $(R, r)$  coordinates has the following form:

$$\begin{aligned}
\hat{H} & = \frac{\left( \frac{e \mathbf{A}(\mathbf{r})}{2c} + \mathbf{p}_r \right)^2}{m} + \frac{\left( \frac{2e \mathbf{A}(\mathbf{R})}{c} + \mathbf{P}_R \right)^2}{4m} + \frac{1}{4} m r^2 \omega_0^2 \\
& \quad + m R^2 \omega_0^2 + \frac{e^2}{\epsilon \mathbf{r}}
\end{aligned} \tag{A.9}$$

Finally, the complete two electron QD Hamiltonian is separated into center of mass Hamiltonian  $H_{CM}$  and relative Hamiltonian part  $H_r$  as shown below:

$$\hat{H} = \hat{H}_{CM} + \hat{H}_r \tag{A.10}$$

$$\hat{H}_{CM} = \frac{1}{2M} \left[ \mathbf{P}_R + \frac{Q}{c} \mathbf{A}(\mathbf{R}) \right]^2 + \frac{1}{2} M \omega_0^2 R^2 \tag{A.11}$$

$$\hat{H}_r = \frac{1}{2\mu} \left[ \mathbf{p}_r + \frac{q}{c} \mathbf{A}(\mathbf{r}) \right]^2 + \frac{1}{2} \mu \omega_0^2 r^2 + \frac{e^2}{\epsilon |\mathbf{r}|} \tag{A.12}$$

Where  $M$  is the total mass =  $2m$ ,  $Q$  is the total charge =  $2e$ ,  $\mu$  is reduce mass =  $\frac{m}{2}$ , and  $q$  is the reduce charge =  $\frac{e}{2}$ .

The center of mass Hamiltonian has the well known harmonic oscillator form for wave function and energy that are given in ref [9]:

$$\begin{aligned}
& \psi_{n_2, m_2}(R) \\
& = (-1)^{n_2} \frac{\beta^{|m_2+1|}}{\sqrt{\pi}} \left[ \frac{n_2!}{(n_2 + |m_2|)!} \right]^{\frac{1}{2}} e^{-\beta^2 R^2 / 2} R^{|m_2|} L_{n_2}^{|m_2|} \beta^2 R^2 e^{i m_2 \phi}
\end{aligned} \tag{A.13}$$

$$E_{CM} = E_{n_{cm}, m_{cm}} = (2n_{cm} + |m_{cm}| + 1) \hbar \sqrt{\frac{\omega_c^2}{4} + \omega_0^2} - m_{cm} \frac{\hbar \omega_c}{2} \tag{A.14}$$

Where  $n_{\text{cm}}, m_{\text{cm}}$  are the radial and angular quantum numbers, respectively,  $L_n^m$  is the associate laguerre polynomial and the parameter  $\beta$  that has the dimensionality of an inverse length is

$$\beta = \sqrt{\frac{m\omega}{\hbar}} \quad \text{and} \quad \omega^2 = \frac{\omega_c^2}{4} + \omega_0^2$$

## Appendix B: properties of the Laguerre polynomials

The following Laguerre relation was used to evaluate the coulomb energy matrix element in a closed form:

$$\int_0^{\infty} t^{\alpha-1} e^{-pt} L_m^{\lambda}(at) L_n^{\beta}(bt) dt = \frac{\Gamma(\alpha)(\lambda+1)_m(\beta+1)_n p^{-\alpha}}{m!n!} \sum_{j=0}^m \frac{(-m)_j (\alpha)_j}{(\lambda+1)_j j!} \left(\frac{a}{p}\right)^j \sum_{k=0}^n \frac{(-n)_k (\alpha+j)_k}{(\beta+1)_k k!} \left(\frac{b}{p}\right)^k \quad (\text{B.1})$$

**Appendix C: the pressure and temperature dependent static dielectric constant and electron effective mass.**

$$\epsilon_r(P, T) = \begin{cases} 12.74 \exp(-1.73 \times 10^{-3}P) \exp[9.4 \times 10^{-5}(T - 75.6)] & \text{for } T < 200 \text{ K} \\ 13.18 \exp(-1.73 \times 10^{-3}P) \exp[20.4 \times 10^{-5}(T - 300)] & \text{for } T \geq 200 \text{ K} \end{cases} \quad (\text{C.1})$$

$$m^*(P, T) = \left[ 1 + 7.51 \left( \frac{2}{E_g^\Gamma(P, T)} + \frac{1}{E_g^\Gamma(P, T) + 0.341} \right) \right]^{-1} m_0 \quad (\text{C.2})$$

$$E_g^\Gamma(P, T) = \left[ 1.519 - 5.405 \times 10^{-4} \frac{T^2}{T+204} \right] + bP + cP^2 \quad (\text{C.3})$$

Where  $m_0$  is the free electron mass,  $E_g^\Gamma(P, T)$  is the pressure and temperature dependent energy band gap for GaAs quantum dots at  $\Gamma$  point,  $b = 1.26 \times 10^{-1} \text{ eV GPa}^{-1}$  and  $c = -3.77 \times 10^{-3} \text{ eV GPa}^{-2}$ .

جامعة النجاح الوطنية  
كلية الدراسات العليا

# تأثير الضغط ودرجة الحرارة على خواص نقطة كمية من (GaAs) منفردة في مجال مغناطيسي

إعداد

فاتن ماهر بزور

إشراف

أ.د. محمد السعيد

د. خالد عليوي

قدمت هذه الأطروحة استكمالاً لمتطلبات الحصول على درجة الماجستير في الفيزياء في كلية  
الدراسات العليا في جامعة النجاح الوطنية - نابلس.

2016



ب

تأثير الضغط ودرجة الحرارة على خواص نقطة كمية من (GaAs) منفردة في مجال مغناطيسي

إعداد

فاتن ماهر بزور

إشراف

أ.د. محمد السعيد

د. خالد عليوي

### الملخص

في هذا العمل تم حساب طاقة المستويات لنقطة كمية من (GaAs) تحت تأثير الضغط الخارجي ودرجة الحرارة والمجال المغناطيسي. تم الحصول على القيم المميزة من خلال حل دالة هاملتون لزوج من الالكترونات في نقطة كمية باستخدام طريقة القطر (Diagonalization). اظهرت النتائج المحسوبة في هذا العمل ان طاقة المستويات للنقطة الكمية تعتمد بشدة على الضغط ودرجة الحرارة. وقد وجدنا أن طاقة المستويات تزداد بزيادة الضغط عند ثبات درجة الحرارة والمجال المغناطيسي وأن طاقة المستويات تقل بزيادة درجة الحرارة وثبات الضغط والمجال المغناطيسي . وقد قمنا أيضا بحساب منحنى الطور الأحادي-الثلاثي للنقطة الكمية. بالاضافة إلى ذلك, قمنا بالتحقق من تأثير الضغط على طاقة الصرف (exchange energy) لنقطة كمية في مجال مغناطيسي. وتظهر المقارنة أن نتائجنا على اتفاق جيد جدا مع النتائج المنشورة.